



DIGITAL ACCESS TO SCHOLARSHIP AT HARVARD

Molybdenum evidence for expansive sulfidic water masses in ~750Ma oceans

The Harvard community has made this article openly available.
[Please share](#) how this access benefits you. Your story matters.

Citation	Dahl, Tais W., Donald E. Canfield, Minik T. Rosing, Robert E. Frei, Gwyneth W. Gordon, Andrew H. Knoll, and Ariel D. Anbar. 2011. "Molybdenum Evidence for Expansive Sulfidic Water Masses in ~750Ma Oceans." <i>Earth and Planetary Science Letters</i> 311, no. 3-4: 264–274.
Published Version	doi:10.1016/j.epsl.2011.09.016
Accessed	February 16, 2015 11:39:17 PM EST
Citable Link	http://nrs.harvard.edu/urn-3:HUL.InstRepos:13041339
Terms of Use	This article was downloaded from Harvard University's DASH repository, and is made available under the terms and conditions applicable to Open Access Policy Articles, as set forth at http://nrs.harvard.edu/urn-3:HUL.InstRepos:dash.current.terms-of-use#OAP

(Article begins on next page)

1 Molybdenum evidence for expansive sulfidic water masses

2 in ~750 Ma oceans

3
4 T. W. Dahl^{1,2,*}, D. E. Canfield^{1,2}, M. T. Rosing^{1,3}, R. Frei^{1,3}, G. W. Gordon⁴, A. H.

5 Knoll⁵, A. D. Anbar⁴

6
7 ¹*Nordic Center for Earth Evolution (NordCEE)*

8 ²*University of Southern Denmark, Campusvej 55, DK-5230 Odense M, Denmark*

9 ³*University of Copenhagen, Øster Voldgade 5-7, DK-1350 Copenhagen K., Denmark*

10 ⁴*School of Earth & Space Exploration, Arizona State University, Tempe, Arizona 85287-*

11 *1404, USA*

12 ⁵*Department of Organismic and Evolutionary Biology, Harvard University, Cambridge,*

13 *Massachusetts 02138, USA*

14
15
16 Final Minor Revisions to accepted version

17 *E-Mail: tdahl@biology.sdu.dk

20 Abstract

21 **The Ediacaran appearance of large animals, including motile bilaterians, is**
22 **commonly hypothesized to reflect a physiologically enabling increase in atmospheric**
23 **and oceanic oxygen abundances (pO_2). To date, direct evidence for low oxygen in**
24 **pre-Ediacaran oceans has focused on chemical signatures in the rock record that**
25 **reflect conditions in local basins, but this approach is both biased to constrain only**
26 **shallower basins and statistically limited when we seek to follow the evolution of**
27 **mean ocean chemical state through time. Because the abundance and isotopic**
28 **composition of molybdenum (Mo) in organic-rich euxinic sediments can vary in**
29 **response to changes in global redox conditions, Mo geochemistry provides**
30 **independent constraints on the global evolution of well-oxygenated environments.**
31 **Here, we establish a theoretical framework to access global marine Mo cycle in the**
32 **past from the abundance and isotope composition of ancient seawater. Further, we**
33 **investigate the ~750 Ma Walcott Member of the Chuar Group, Grand Canyon,**
34 **which accumulated in a rift basin with open connection to the ocean. Iron speciation**
35 **data from upper Walcott shales indicate that local bottom waters were anoxic and**
36 **sulfidic, consistent with their high organic content (up to 20 wt%). Similar facies in**
37 **Phanerozoic successions contain high concentrations of redox-sensitive metals, but**
38 **in the Walcott Member, abundances of Mo and U, as well as Mo/TOC (~ 0.5**
39 **ppm/wt%) are low. $\delta^{98}\text{Mo}$ values also fall well below modern equivalents**
40 **($0.99\pm 0.13\text{‰}$ versus $\sim 2.35\text{‰}$ today). These signatures are consistent with model**
41 **predictions where sulfidic waters cover ~1-4% of the global continental shelf area,**
42 **corresponding to a ~400-800 fold increase compared to the modern ocean.**

43 **Therefore, our results suggest globally expansive sulfidic water masses in mid-**
44 **Neoproterozoic oceans, bridging a nearly 700 million-year gap in previous Mo data.**
45 **We propose that anoxic and sulfidic (euxinic) conditions governed Mo cycling in the**
46 **oceans even as ferruginous subsurface waters re-appeared 800-750 Ma, and we**
47 **interpret this anoxic ocean state to reflect a markedly lower atmospheric and**
48 **oceanic O₂ level, consistent with the hypothesis that pO₂ acted as an evolutionary**
49 **barrier to the emergence of large motile bilaterian animals prior to the Ediacaran**
50 **Period.**

51 **Keywords:** Earth history, Mo isotopes, stable isotope fractionation, molybdenum, paleo-
52 redox, Chuar Group, Grand Canyon, Neoproterozoic, black shales, anoxic environments,
53 euxinia.

54

55 **1 Introduction**

56 Most evidence suggests that the atmosphere contained essentially no O₂ prior to
57 the so-called "Great Oxidation Event" (GOE) 2.45-2.3 Ga [1, 2]. A variety of chemical
58 proxies signal a rise in atmospheric O₂ concentrations at this time [2, 3], although to
59 levels which probably remained well below present concentrations [4, 5]. Current models
60 propose higher atmospheric oxygen levels promoted increased continental weathering of
61 sulfide to sulfate, increasing the flux of sulfate to the ocean and stimulating marine
62 sulfide production by sulfate reduction in low oxygen bottom waters. Increased sulfide
63 production led to the expansion of sulfide into broad regions of the global ocean [6],
64 perhaps especially in oxygen-minimum zone (OMZ) settings [7]. Mo chemistry provides
65 a potentially powerful way of evaluating the history of euxinic water masses, because Mo

66 reactivity and Mo burial rate dramatically increase in the presence of H₂S. However,
67 available analyses remain limited and no data have been reported for rocks deposited
68 between 1400 and 663 Ma.

69 Black shales of the ca. 800-750 Ma Chuar Group, Grand Canyon, provide an
70 opportunity to bridge this gap, allowing insight into a critical time in Earth history during
71 or just before the onset of major Neoproterozoic cooling [8]. Chuar deposition coincides
72 with an expansion in the diversity of fossil protists [9] and also corresponds to some
73 molecular clock estimates for the initial divergence of animals from their closest
74 protozoan sister groups [10]. Evidence presented here suggests that during upper Walcott
75 time the marine Mo cycle was controlled by widespread sulfidic water masses that would
76 have persisted under much lower marine pO₂ than today. These results support the
77 hypothesis that O₂ remained low in the oceans and atmosphere at times before
78 macroscopic, motile bilaterian animals evolved in marine ecosystems.

79

80 **1.1 Molybdenum as a paleoenvironmental proxy for H₂S**

81 Molybdenum is a redox sensitive element: it enters the oceans mainly as dissolved
82 MoO₄²⁻, and has done so for billions of years since the onset of oxidative weathering
83 [11]. The accumulation of Mo in the modern oceans is largely dictated by the high
84 solubility of the MoO₄²⁻ species and its slow removal rate in the presence of dissolved
85 O₂. The slow rate of oxic removal is a result of the very low reactivity of molybdate, with
86 removal taking place as a rare Mo species (e.g. polynuclear Mo₆O₁₉²⁻ [12]) in seawater
87 adsorb onto precipitating Fe-Mn-oxides [13, 14]. In contrast, molybdate reacts to form

88 particle-reactive oxythiomolybdates in the presence of $>10 \mu\text{M}$ aqueous H_2S [15] and is
89 actively scavenged onto particulate matter in anoxic and sulfidic (= euxinic) waters [16].

90 The Mo accumulation rate in sulfidic settings (whether sulfide is retained in pore
91 waters or in the water column) is 100-1000 fold higher than in present day oxic ocean
92 waters (see [17] and references therein). Today, 30-50% of oceanic Mo removal occurs
93 into sediments with sulfidic pore fluids and mildly reducing overlying waters typical of
94 some OMZs. Due to the vast areas of oxic seafloor in the modern deep oceans, oxic
95 ferromanganese crusts remove 35-50% of the oceanic input, with the remaining 5-15%
96 buried under highly sulfidic water columns (e.g. Cariaco Basin, Baltic Sea, Black Sea,
97 Namibian Shelf). Because oxic conditions dominate in the ocean today, Mo removal is
98 slow, resulting in relatively high Mo concentrations in seawater (105 nM, greater than
99 any other transition metal). Accordingly, Mo has a long residence time in the modern
100 ocean ($\tau_{\text{Mo}} \sim 800$ kyrs; [18]) relative to ocean mixing time scales (1.5 kyr, [19]). This
101 means that Mo in any marine basin tracks average global conditions and would have done
102 so in the past provided contemporaneous oceans were also well mixed with respect to
103 molybdenum.

104 Molybdenum accumulates with organic matter in sediments of modern marine
105 euxinic basins. The role of organic matter in euxinic Mo burial is currently debated [20].
106 Organic matter may add ballast to Mo adsorbed onto FeS particles and allow Mo
107 transport out of the water column, Mo-S compounds may also be deposited with sulfate
108 reducing bacteria [21-23], or both. In any case, sedimentary Mo-TOC correlations have
109 been used to infer Mo concentrations in local basins [24]. This is because low Mo/TOC is
110 characteristic of sediments underlying stagnant, sulfidic waters where Mo removal is

111 nearly complete (Black Sea) and Mo recharge is slow. In contrast, high Mo/TOC is
112 associated with rapid water exchange with the ocean and significant water column sulfide
113 (e.g. Namibian shelf, modern Saanich Inlet and the Cariaco Basin). Maximum Mo/TOC
114 values at any given time are set by the Mo concentration of global seawater at the time of
115 deposition. Available sedimentary Mo/TOC ratios suggest that the average value [17] has
116 increased through Earth history in concordance with increasing seawater Mo
117 concentrations and $\delta^{98}\text{Mo}$ in more oxygenated oceans [5].

118 Because its residence time is long relative to modern ocean mixing time scales,
119 Mo has a uniform isotopic composition in seawater (SW) which is $\delta^{98}\text{Mo}^1 = 2.3 \pm 0.1\text{‰}$ in
120 the present oceans. This value is isotopically heavier than the $\sim 0.7\text{‰}$ value of the input to
121 the oceans, because oxic (OX) and other non-euxinic sediments preferentially scavenge
122 light Mo isotopes with a large fractionation from the seawater value (e.g. $\Delta_{\text{OX-SW}} = -$
123 2.9‰ [13, 14]). Conversely, little or no isotope fractionation is expressed during Mo
124 removal into highly euxinic sediments (EUX) with $\text{H}_2\text{S} > 10 \mu\text{M}$ [16, 25]. Therefore,
125 $\delta^{98}\text{Mo}$ in such sediments can reflect seawater composition. At intermediate redox
126 conditions, where Sulfide Accumulates at Depth inside the sediments (SAD), Mo is
127 retained with an isotopic offset from seawater of roughly $\Delta_{\text{SAD-SW}} \sim -0.7\text{‰}$ [26].
128 Consequently, $\delta^{98}\text{Mo}_{\text{SW}}$ also reflects the balance between how much Mo is buried in
129 highly euxinic (EUX, no fractionation) versus Mo buried in oxic (OX and SAD,
130 fractionated) bottom waters. Oxygenated oceans have high $\delta^{98}\text{Mo}_{\text{SW}}$, while low $\delta^{98}\text{Mo}_{\text{SW}}$
131 values approaching the oceanic input value imply expanded oceanic euxinia. A major
132 drop in seawater Mo concentrations accompanies the latter.

133

134 **1.2 Model: Relating Mo and $\delta^{98}\text{Mo}_{\text{SW}}$ in ancient seawater to euxinic seafloors**

135 We provide a framework to quantify the extent of euxinic seafloor from models of
136 the ancient Mo cycle based on our current understanding of how the modern Mo cycle
137 works. By definition and in contrast to local redox indicators, we cannot directly calibrate
138 global proxies in modern local environments (e.g. lakes). Instead, we rely on quantitative
139 modeling of the global marine Mo cycle and assume that known removal processes also
140 operated in the past. Here, we illustrate the steady-state behavior of the marine Mo cycle
141 by a 1-box model, where riverine and hydrothermal sources balance removal into oxic
142 (OX), mildly reducing (SAD) and euxinic (EUX) sinks:

143

144 equation 1
$$\text{dMo}/\text{dt} = F_{\text{sources}} - F_{\text{sinks}}$$

145 equation 2
$$F_{\text{SINKS}} = F_{\text{OX}} + F_{\text{SAD}} + F_{\text{EUX}}$$

146

147 Today, Mo is sourced into the ocean mainly as dissolved MoO_4^{2-} by rivers ($1.8 \cdot 10^8$
148 moles yr^{-1}) and hydrothermal sources ($0.2 \cdot 10^8$ moles yr^{-1}) and the export pathways are
149 grouped into three distinct redox environments, as outlined above [27, 28].

150

151 The model can be used to constrain the areal extent of each of these redox
152 environments. We scale the removal fluxes in each sink to their respective seafloor
153 coverage (A_i):

154

¹ $\delta^{98}\text{Mo} = [(^{98}\text{Mo}/^{95}\text{Mo})_{\text{sample}} / (^{98}\text{Mo}/^{95}\text{Mo})_{\text{standard}} - 1] \cdot 1000$. There is still no certified standard, so results are given relative to our in-house ICP standard Mo solution (Alfa Aesar Specpure Lot# 802309E).

155 equation 3 $F_i = A_i \cdot r_i$, where $i = \text{OX, SAD, or EUX}$.

156

157 The burial rates in oxic sediments, sulfidic sediments and euxinic settings must be
158 self-regulated, otherwise the oceanic Mo inventory would either vanish or accumulate
159 infinitely when sinks expand or shrink. We adopt a self-regulated feedback between
160 removal fluxes (F) and marine Mo inventory (M), $F_i \sim M^{y_i}$. The end member cases $y_i =$
161 1 and $y_i = 0$ correspond, first, to a direct feedback and, second, to the unrealistic case of
162 no self-regulation, respectively.² Each redox environment may operate with its own
163 response function, $y_i > 0$. However, the direct feedback model, $y = 1$, is attractive because
164 it matches expectations, if removal rates were limited only by diffusive or advective
165 transport into the sulfidic waters. In this case, the burial rate in the i^{th} sink is proportional
166 to oceanic Mo inventory:

167

168 equation 4 $r_i = r_{i,\text{today}} \cdot \text{Mo}/\text{Mo}_{\text{today}}$

169

170 A mathematical derivation of the solution can be found in the supplementary online
171 material (section A2.2.2.1).

172

173 *1.2.1 Mo concentration and residence time for the direct feedback model, $y = 1$:*

² A stronger feedback $y > 1$ is possible if seawater Mo concentration limits Mo export in more than one manner. For example, if both the rate of Mo supply and particle rain rate (controlled by primary production) is decreasing due to Mo limited supply [29] A.D. Anbar, A.H. Knoll, Proterozoic ocean chemistry and evolution: A bioinorganic bridge?, Science 297(2002) 1137-1142. Here, we adopt the simplest feedback with a direct response between fluxes and oceanic inventory, $y = 1$, and assume the same feedback operates today. Even this fast removal feedback, we will see, is not enough to drive open ocean Mo concentrations below the thresholds where nitrogen fixation can limit global primary production, and thus $y > 1$ becomes hard to envision.

174 An important feature of the direct feedback model is that all reasonable choices of
175 parameter values with euxinic shelves (<8% seafloor) lead to long marine residence time
176 scales (>30,000 years) compared to ocean mixing time scales (~1,500 yr [19]). Hence,
177 Mo should be well mixed in the open ocean under these circumstances even if mixing by
178 global ocean circulation proceeded at a rate ~10 times slower than today. We note that
179 burial rates in the deep ocean are greatly exaggerated in this model, since we have scaled
180 mean accumulation rates to data obtained from shelf environments, where bulk
181 sedimentation rates are much greater. Thus, Mo drawdown in each sink is exaggerated,
182 leading us to overestimate Mo drawdown upon expansive euxinic seafloor, and
183 conversely to underestimate euxinic coverage for a given Mo drawdown. The true Mo
184 residence time would actually be longer than predicted by our simplistic model.

185

186 The isotopic composition of Mo provides independent constraints on the global
187 Mo budget. The steady state solution to isotopic mass balance in the global ocean reads:

188

189 equation 5
$$\delta_{IN} = f_{OX} (\delta_{SW} - \Delta_{OX}) + f_{SAD} (\delta_{SW} - \Delta_{SAD}) + (1-f_{SAD} - f_{OX}) (\delta_{SW} -$$

190
$$\Delta_{EUX})$$

191

192 where f_{OX} and f_{SAD} is the fraction of total Mo removed into oxic and SAD settings,
193 respectively. δ_{IN} is the isotopic composition of oceanic input, δ_{SW} is the isotopic
194 composition of contemporaneous seawater, Δ_i are fractionations into their respective
195 sinks.

196

197 Quantitative assessments depend on how well we understand fractionation in the
198 contemporaneous ocean and the $\delta^{98}\text{Mo}$ of the oceanic input. The full range of possible
199 oceanic steady states can be explored if we keep the oceanic input flux constant at
200 modern rates and assume fractionation into major sinks similar to modern values.
201 Riverine inputs discharge 90% of all Mo [30] with an average $\delta^{98}\text{Mo}$ of $\sim 0.7\text{‰}$ [31-33].
202 This is indistinguishable from average molybdenite deposits, at $0.4\pm 0.5\text{‰}$, which we
203 argue resemble the average crustal composition (further discussion in section below).
204 Therefore, we assume that the average $\delta^{98}\text{Mo}$ of oceanic input on > 1 Myr time scale was
205 the same as today. Model results for seawater Mo inventory and $\delta^{98}\text{Mo}$ at various degrees
206 of expansive euxinia are summarized in Table 1.

207

208 **1.3 Mo isotope fractionation on land and in rivers**

209

210 In early studies, the crustal average isotopic composition of Mo was reported at $\sim 0\text{‰}$
211 based on two granite samples [34, 35], and this has been taken as the canonical value ever
212 since. If correct, the isotopic offset between crust and dissolved Mo in rivers implies that
213 there is an additional reservoir of isotopically fractionated Mo in nature. Here, we offer a
214 simpler explanation consistent with current observations and advocate that average
215 crustal composition is, indeed, very close to average dissolved load in rivers.

216

217 Crustal samples display significant variability with the two reported granite samples
218 representing the lighter side of the crustal distribution around $\sim 0\text{‰}$, with subduction-
219 related volcanics at higher values $0.9\pm 0.3\text{‰}$ [34]. We suggest that average crustal Mo

220 isotope composition is more accurately (but not precisely) represented by the most
221 concentrated Mo-phase in the crust, namely molybdenite (a view also held by [35]). We
222 argue that molybdenite probably formed under conditions with efficient Mo accumulation
223 and, likely, wholesale Mo capture and little or no net isotope fractionation relative to its
224 crustal source. Molybdenites carry $\delta^{98}\text{Mo}$ compositions $0.36 \pm 0.54\text{‰}$, 1-standard
225 deviation of the mean, $n = 86$ (Figure 1) with some of the variability reflecting Rayleigh
226 distillation during vapor transport and precipitation in single molybdenite occurrences
227 [36].

228

229 An alternate hypothesis states that the riverine Mo has a higher $\delta^{98}\text{Mo}$ than crustal rocks
230 supply to rivers. Such isotope fractionation between crustal rocks and dissolved Mo in
231 rivers has been proposed to govern major changes in the isotopic composition of the
232 oceanic input over geological time [31, 32]. Mo bound to Fe-oxyhydroxide particles in
233 rivers and soils is argued to hold the lighter Mo isotopes [31, 32]. However, there are two
234 issues to consider before such a hypothesis can be accepted: 1) Is the reservoir large
235 enough? 2) Is the isotope composition of the fractionated sink low enough to account for
236 the apparent 0.7‰ offset between crust and rivers?

237

238 In world rivers, the particulate fraction (presumably carrying lower $\delta^{98}\text{Mo}$ than dissolved
239 Mo) is a minor constituent accounting for less than 5% of the total oceanic inputs [4-6%
240 [37]; 1-2% [31]]. If the average crustal value was 0‰ , then the particulates associated
241 with river flux should be fractionated 12‰ - approximately ten-fold higher than can be
242 generated by any known process [14, 38]. Observations are limited, but the Mo adsorbed

243 onto Fe precipitates and colloidal Mo in one Icelandic river is fractionated by -0.6‰ and
244 -0.8‰ relative to dissolved Mo, respectively [32]. At the observed fractionation, these
245 particles could shift the average crustal value only -0.05‰ relative to the dissolved
246 riverine input.

247

248 The amount of Mo retained in soils is only ~7% of the dissolved inventory in the oceans
249 (Estimate: $[\text{Mo}]_{\text{soil}} = 3 \text{ ppm}$, $\rho_{\text{soil}} = 1.5 \text{ g cm}^{-3}$, average global soil thickness = 1.5 m).
250 Hence, the residence time of Mo in modern soils is only ~60,000 years, and likely was
251 much shorter in the Neoproterozoic, so variations in the magnitude and isotopic
252 composition of this reservoir could only be observed in marine sediments on similar or
253 shorter time scales. The Walcott Member of the Chuar Group was deposited over > 1
254 million years [39], so we are looking at the average state of many oceanic Mo residence
255 times, where soil-modulated effects vanish. Over long time scales, average oceanic input
256 will match the $\delta^{98}\text{Mo}$ of average crust with small variability around crustal average, but
257 substantial variability (~1.5‰) could exist between individual rivers [31]. If the isotopic
258 composition of oceanic input were different from today, any differences must have been
259 caused by variation in a much larger Mo terrestrial reservoir, of which there is no
260 evidence. For these reasons, we constrain our models for the molybdenum cycle at 750
261 Ma using same oceanic input as today.

262

263 **2 Geological settings and environmental conditions in the Walcott basin**

264 The Chuar Group was deposited in an intracratonic rift basin at near-equatorial
265 (2°S to 18°N) latitudes [40] during the break-up of the supercontinent Rodinia [41]. The

266 ~1600 m thick succession is subdivided into the Kwagunt and underlying Galeros
267 formations (Figure 2) [39]. We examined carbonaceous shales in the uppermost ~250
268 meters of the Walcott Member, Kwagunt Formation. Samples were collected from
269 outcrops in the Sixty-Mile Canyon and the NE Flank of Nankoweap Butte [42].

270 The Walcott Member is capped by an ash layer hosting zircons with a U-Pb age
271 of 742 ± 6 Ma [41]. The bottom of the Galeros Formation, some 1400 meters lower in the
272 Chuar succession, contains authigenic monazite with a U-Pb age of ca. 770 Ma [43],
273 consistent with both the presence of *Cerebrosphaera buickii* [44], an acritarch
274 stratigraphically restricted to sediments younger than 777 ± 7 Ma in the Adelaide Rift
275 Complex [45] and some 300 stacked, meter-scale cycles of sandstone-capped dolomite,
276 each thought to represent ~100,000 yrs [39].

277 The Chuar Basin was marine and had contact to the open ocean, as recorded both
278 by sedimentological and paleontological evidence. Sedimentary structures suggest a wave
279 and tide-influenced depositional system that would not exist in lacustrine or highly
280 restricted settings [39] (Figure 2). Microfossils in the Walcott Member belong to taxa
281 found widely in 800-750 Ma successions around the world [44], providing independent
282 evidence that at least surface waters exchanged with the global ocean.

283 Previous studies have concluded that most carbonaceous shales of the Walcott
284 Member accumulated beneath sulfidic subsurface waters [7, 46]. In contrast, the lower
285 Chuar shales were deposited beneath water masses that were commonly anoxic but
286 ferruginous [7]. It is inferred that the water column was structured such that sulfidic
287 subsurface waters, perhaps quite extensive, developed when rates of export production
288 were high. With the exception of a few samples (AK-10-53-12, AK-10-60-16) most

289 Chuar samples display low Fe-oxide contents despite abundant highly reactive iron,
290 indicating that post-depositional oxidative weathering has been minimal [7].

291

292 **3. Methods**

293 Rock samples were crushed in a ceramic mortar. Total organic carbon (TOC)
294 content was determined at University of Southern Denmark using a FLASH 2000
295 Element Analyzer interfaced through a ConFlo IV to a Thermo Scientific Delta V
296 Advantage Continuous Flow Isotope Ratio Mass Spectrometer. Samples were first acid-
297 leached in 2M HCl for >24 hours to remove carbonate. Conversion from intensity to
298 concentrations was done using a certified Nicotinalamide standard from Thermo Electron
299 S.p.A. (Lot O13A), measured at four different intensities. The procedural TOC blank was
300 measured by analyzing a pure silicate quartz powder and was well below the
301 concentration of the lowest standard (corresponding to <<0.4wt%). Fe speciations were
302 previously determined using a validated extraction method [46]. For trace metal
303 concentration analyses, samples were ashed at 550°C for 12 hours and rock powders were
304 then weighed into Teflon vials and digested using a 5:1 mixture of conc. HF and conc.
305 HNO₃ for 48 hours. After evaporation the samples were dissolved in concentrated HCl
306 for 24 hours, dried, and finally re-dissolved in 6M HCl. Sample aliquots for concentration
307 analyses were first dried and re-dissolved in nitric acid before dilution with MQ H₂O, so
308 that the analyses could be done in 2% HNO₃ solutions using a quadropole ICP-MS
309 (Thermo Elemental X-Series with Collision Cell Technology) at Arizona State
310 University. A continuous supply of internal standard (Ge, Y, In, Bi) was mixed online
311 into the sample during analysis, and the response of this solution was monitored to

312 correct for plasma suppression. The conversion from intensity to concentrations was done
313 by comparison to a known multi-element standard made from single element ICP
314 solutions with elemental concentrations optimized for black shales measured at four
315 different intensities. A standard curve was measured before, during and after the samples
316 to compensate for drift in the observed values.

317

318 For isotopes, Mo was purified from the matrix by techniques described in [35] and
319 isotope ratios determined by MC-ICP-MS (Thermo Elemental Neptune) at Arizona State
320 University in the W.M. Keck Foundation Laboratory for Environmental
321 Biogeochemistry. We used Zr-doping to correct for instrumental mass bias and applied
322 quality controls described in [16]. An aliquot of the sample taken before and after the
323 purification procedure was measured to ensure quantitative chemical recovery (>92%)
324 during ion exchange purification which could otherwise change the isotope composition
325 of the eluent. The long-term external reproducibility of $\delta^{98}\text{Mo}$ (2 standard deviation) of a
326 rock standard (SDO-1) was better than $\pm 0.15\%$ [47].

327

328 **4. Results**

329 Data are summarized in Table 2. Fe speciation data from the Walcott Member show clear
330 enrichment of highly reactive iron ($\text{Fe}_{\text{HR}}/\text{Fe}_{\text{T}} \sim 0.8$) relative to oxic sediments and
331 riverine particulates (<0.38 , [48]). In most of the Walcott shales, pyrite accounts for the
332 majority of highly reactive iron found in the Walcott shales ($\text{Fe}_{\text{P}}/\text{Fe}_{\text{HR}} \sim 0.5-0.9$) (Figure
333 3). A few Fe-carbonate rich samples are found in the middle of the Walcott section (AK-
334 10-60-31, AK-10-60-32) near paleo-subaerial exposure surfaces. The highly reactive iron

335 in the top-most sample and in samples from the very bottom of the Walcott member
336 consists mainly of Fe-oxides. Overall, Mo and U concentrations are remarkably low, at 1-
337 12 ppm and 1-7 ppm, respectively. This translates into small, but significant, average
338 enrichment factors above average crust, Mo $EF_{Al} = 6$ and U $EF_{Al} = 4$; see figure 3
339 caption for definition of enrichment factors. Samples enriched in highly reactive iron
340 (Fe_{HR}/Fe_T) are also consistently enriched in total iron relative to continental crust (Fe
341 EF_{Al}). The $\delta^{98}Mo$ composition of Walcott shales, both with a strictly euxinic ($Fe_P/Fe_{HR} >$
342 0.8) and with a probable euxinic ($Fe_P/Fe_{HR} > 0.5$) Fe speciation signature (figure 3), are
343 rather constant at $0.97 \pm 0.16\text{‰}$ ($n=4, 1\sigma$), and $0.99 \pm 0.13\text{‰}$ ($n=6, 1\sigma$), respectively. The
344 $\delta^{98}Mo$ of the authigenic component can be derived, assuming that the lithogenic
345 component is represented by either average crustal value (0.4-0.7‰, Figure 1) or from
346 samples with little or no authigenic enrichment ($\delta^{98}Mo \sim 0.8\text{‰}$), which leads to
347 authigenic Mo with $\delta^{98}Mo$ of 1.25 ± 0.40 and 1.10 ± 0.30 , respectively. The average bulk
348 $\delta^{98}Mo$ value of ferruginous sediments, $0.80 \pm 0.09\text{‰}$ ($n=3, 1\sigma$) is within error
349 indistinguishable from the euxinic samples. The samples from the top and bottom of the
350 section with large proportions of Fe-oxides display lower $\delta^{98}Mo$ values, indicative of
351 isotope fractionation. Particularly, one sample (AK-10-53-12), distinctly enriched in Mo
352 (12 ppm), shows a remarkably low $\delta^{98}Mo$ of 0.2‰.

353

354 **5. Discussion**

355 Previous studies have used **local** paleoenvironmental indicators with short marine
356 residence times relative to oceanic mixing time to describe redox conditions in the
357 Walcott basin, finding evidence for deposition in a basin with anoxic and sulfidic bottom

358 waters (Figure 2 and 3 [7, 46]), Here, Mo chemistry is used to target the **global** extent of
359 anoxic and sulfidic water masses in the contemporaneous oceans.

360 In persistently euxinic water columns, Mo and U concentrations are typically high
361 (Table S2), but they are unusually low in euxinic Walcott samples. These values reflect
362 far less metal enrichments relative to crustal average than in previously analyzed Meso-
363 to Neoproterozoic black shales (~24 ppm Mo [11, 17], >10 ppm U [49]) and are
364 reminiscent of typical Archean sediments (~3.3 ppm Mo [17], <10 ppm U [49])
365 interpreted as reflecting low marine metal inventories associated with extensive anoxic
366 and sulfidic removal pathways. An increase in Mo and U enrichment towards the end of
367 the Neoproterozoic [17, 49] is consistent with the growth of oceanic metal inventories as
368 oxic water masses expanded [5, 17].

369 Walcott shales contain 2-20 wt% organic carbon [41, 42], corresponding to
370 average Mo/TOC ~ 0.4 ppm/wt% in the euxinic shales. Similar low Mo/TOC values have
371 been suggested to record <5 nM Mo in the water column [17, 50]. This is an order of
372 magnitude lower than the Proterozoic average of 6.4 ppm/wt% between 1700-550 Ma,
373 which may represent seawater Mo concentrations of ~20 nM [17].

374 $\delta^{98}\text{Mo}$ shows little systematic variation with sedimentary Mo EF (Figure 4), but
375 the data are completely consistent with mixing between a lithogenic component with
376 riverine discharge at an average crustal $\delta^{98}\text{Mo}$ of 0.4-0.7‰ and a marine end member
377 value of ~1.0‰. This marine value is only marginally enriched in $\delta^{98}\text{Mo}$ over the modern
378 riverine value and lies well below modern seawater at 2.3‰. Two samples in the middle
379 of the section with high Fe-carbonate content coincide with sedimentological evidence
380 for subaerial exposure and may reflect a brief interval of ferruginous and non-euxinic

381 deposition. The Fe_P/Fe_{HR} indicator gives a rough estimate of local water column
382 conditions and is not tuned for firm conclusions about the samples with ratios in the 0.5-
383 0.8 range, which have been deposited in either a euxinic basin or under ferruginous
384 waters with sulfidic sediments. However, the samples near exposure surfaces display
385 $Fe_P/Fe_{HR} = 0.2-0.3$, indicative of sulfate reduction, but display no isotope fractionation
386 relative to euxinic shales and contemporaneous seawater. Two anoxic samples at the top
387 of the section (AK10-53-12, AK-10-53-13) have suffered from post-depositional
388 oxidation ($Fe_{OX}/Fe_{HR} = 0.9-1.0$) with the former clearly fractionated from the mixture of
389 lithogenic and authigenic Mo defined by the rest of the samples (Figure 4). This
390 fractionated sample is particularly interesting, since its high Fe oxide content may result
391 from late oxic diagenesis/weathering. Its high Mo content is still modest in comparison to
392 the Proterozoic average, and its Mo enrichment ($Mo_{EF} = 12.5$) compares to neighboring
393 samples ($Mo_{EF} < 30$) in the uppermost Walcott section. Hence, we cannot rule out that
394 Mo isotope fractionation occurred during diagenetic alteration in this case. In any event,
395 the small amount of isotopic variation through ~100 meters of Walcott shales suggests
396 consistently sulfidic bottom-water chemistry (as reported also in previous studies [7, 46])
397 and quantitative scavenging from a Mo-depleted water column with an estimated $\delta^{98}Mo$
398 of $1.0 \pm 0.1\%$.

399

400 **5.1. Expanded sulfidic water masses at ~750 Ma**

401 We have tested three hypotheses to account for the low sedimentary Mo
402 concentrations, the low Mo/TOC ratios and $\delta^{98}Mo$ values in the Walcott shales. These
403 models include: 1) deposition in a hydrographically isolated basin with Mo

404 concentrations and $\delta^{98}\text{Mo}$ values distinct from the open ocean, 2) incomplete Mo
405 scavenging in the Walcott basin, and 3) globally expanded euxinic water masses with
406 globally low [Mo] and $\delta^{98}\text{Mo}$ in seawater.

407 Hypothesis 1 can be rejected from paleontological, hydrodynamic, and
408 geochemical considerations. The Walcott shales contain a globally a significant marine
409 microfossil assemblage, as well as sedimentological evidence of relatively high water
410 stand during Walcott times, pointing to maximal ocean-to-basin water exchange. In light
411 of the low Mo concentration and the $\delta^{98}\text{Mo}$ data, it is inconceivable that hydrodynamic
412 restriction would explain the data if a modern Mo cycle operated in the open ocean,
413 because that would imply that only 1% of the water entering the Chuar Basin was
414 sourced from the ocean, with the remaining 99% originating as fresh water from local
415 rivers. Such a hydrographic situation is incompatible with even the most restricted
416 estuaries today. Furthermore, sulfur isotope fractionation between carbonate associated
417 sulfate and pyrite within the basin implies sulfate levels above $\sim 200 \mu\text{M}$ sulfate [51],
418 requiring a substantial flux of water from the open ocean. This is because rivers carry too
419 low a sulfate concentration ($\sim 50 \mu\text{M}$ in unpolluted modern rivers) to account for the
420 significant S isotope fractionation found in the basin, if they were also the major source
421 of water (further details in the supplement).

422 Hypothesis 2 can be rejected on the basis of comparisons with modern low-sulfide
423 basins and estimates of the H_2S concentration in the Chuar basin (see supplementary
424 online material for details). There are at least two prerequisites for rapid euxinic Mo
425 removal: H_2S levels sufficiently high to form particle-reactive oxythiomolybdates [15,
426 16], FeS formation in the water column [20] and/or other sinking particles. Both organic

427 matter and iron sulfides (FeS and FeS₂) settled out of the Chuar water column, as the
428 Walcott shales contain >2 wt% total organic carbon and high proportions of pyrite
429 (Fe_P/Fe_{HR} > 0.8). Reactive MoOS₃²⁻ and possibly MoS₄²⁻ (given enough time) are slowly
430 produced from molybdate in the presence of >10 μM H₂S. The high pyrite content is
431 evidence that amorphous FeS formed in the basin through the reaction of Fe²⁺ with HS⁻.
432 From this, we estimate that >2 μM H₂S (and >7 μM ΣS(-II) = H₂S + HS⁻ + S²⁻ at pH =
433 7.69, T = 8°C [52]) was permanently available in the deep-water column, and that
434 concentrations might have been as high as the sulfate concentrations in contemporaneous
435 surface seawater ~1,000-4,000 μM [7, 53]. These sulfide estimates are higher than
436 observed even in intermittently euxinic settings such as the Benguela upwelling system
437 off the coast of Namibia, where temporal emission of hydrogen sulfide [54], is sufficient
438 to activate rapid scavenging of Mo and produce sedimentary Mo concentrations of 30-50
439 ppm [55].

440

441 Recently, Helz et al. [20] proposed a new model for euxinic Mo removal that not only
442 requires H₂S, but also moderate pH. Mo precipitation would be hindered at pH > 8,
443 provided >1000 μM ΣS(-II) (H₂S > 100 μM, T = 20°C). Sulfate reduction causes
444 seawater pH to decrease relative to the surface ocean, with values of 7.1-7.7 in the
445 deepest parts of modern euxinic basins (see summary in [20]). Hence, pH-inhibition of
446 the hypothesized Mo removal process could occur if seawater pH were substantially
447 higher than today and total sulfide concentration were near the maximal value.
448 Nonetheless, Mo precipitation should still proceed at the chemocline. With this in mind,
449 we conclude that the Walcott basin was most likely capable of efficient Mo scavenging at

450 times of either maximum or minimum euxinia (e.g. $Fe_P/Fe_{HR} > 0.8$, and >0.5 ,
451 respectively). Still, the Mo enrichment is remarkably small.

452 Hypothesis 3 provides the best explanation for the data, implying globally
453 expansive euxinia at ~750 Ma. Severe euxinia in the world ocean is sufficient to explain
454 the data, but a combination of global anoxia and basinal restriction is favored and would
455 easily fit the exceptionally low [Mo] and $\delta^{98}Mo$ in the Walcott member and rather low
456 values in other Proterozoic successions [56, 57]. We explore this solution further using
457 the simple model presented above (section 1.2) to interpret the oceanic Mo cycle 750
458 million years ago.

459

460 **5.2 Marine Mo cycle at 750 Ma**

461

462 If the $\delta^{98}Mo$ of seawater during Walcott times was steady at $1.0 \pm 0.1\%$, we can
463 derive permissible solutions to the Mo budget. The proportion of euxinic Mo removal can
464 be assessed by first investigating end member cases. Ignoring the oxic removal pathway,
465 simple two sink mass balance predicts that euxinic sinks accounted for $66 \pm 10\%$ of
466 oceanic Mo removal (equation 5), with the rest in SAD settings (using $\Delta_{SAD} = -$
467 $0.7 \pm 0.2\%$, $\Delta_{EUX} = 0\%$). A more prominent euxinic sink would result if removal pathways
468 with higher fractionations, such as oxic sediments, were important. For example, we find
469 90% euxinic removal if we ignore the SAD sink and posit only oxic and euxinic Mo
470 burial. In these cases, the euxinic removal pathway would have operate an order of
471 magnitude faster than today (5-15%, [17, 26, 56]).

472

473 Our model (section 2) using all three major Mo sinks leads to a range of possible
474 solutions for the mean ocean concentration and isotopic composition of Mo at ~750 Ma
475 (Table 1). The condition in which euxinic water masses cover 2-4% of the global seafloor
476 satisfies a seawater $\delta^{98}\text{Mo}$ of $1.0\pm 0.1\%$ and predicts 7-20 nM Mo in seawater, consistent
477 with averages deduced from Mo/TOC data for Proterozoic samples [17]. This represents
478 a 400-800 fold expansion of euxinic areas in Chuar times compared to today (~0.05%
479 seafloor), and it necessitates sulfidic water masses beyond restricted fjords and inland
480 basins. That is, to satisfy observed geochemical data, one has to postulate sulfidic
481 oxygen-minimum zones in the open ocean, e.g. on the continental shelves. The model
482 predicts a Mo residence time of 50-200 kyrs - long enough that open oceans would have
483 carried a uniform isotope composition, even if ocean mixing time scales were
484 substantially slower than today (~1.5 kyrs).

485 We view our model results as illustrative but only semi-quantitative, as we have
486 assumed that average modern removal rates apply to very different ancient environments.
487 For example, if euxinia extended into low sedimentation rate deep-sea environments,
488 there would be little influence on the isotope mass balance. We can conclude, however,
489 that since oxic removal pathways were likely limited during the time of Chuar deposition
490 [7, 46], the removal of Mo into euxinic environments was substantial, and euxinic
491 environments were much more abundant than today.

492

493 **5.3 Implications for nutrient limitation in Proterozoic oceans**

494 Molybdenum scarcity has been hypothesized to have limited primary production
495 in the Proterozoic ocean because nitrogen fixation is most efficient with Mo-based

496 nitrogenase enzymes [29]. Our model results allow us to assess this issue further, since
497 limited pure culture experiments indicate that nitrogen fixation rate is reduced at <2 nM
498 Mo, but not at 5 nM [58, 59]. Assuming that our model parameterization is valid and that
499 the culture experiments apply to the marine system, one would infer that Mo was not
500 sufficiently scarce to limit primary production in the open oceans at 750 Ma. The model
501 suggests that Mo-limited nitrogen fixation in open ocean settings is linked to a reduced
502 oxic weathering regime reminiscent of the Archean atmosphere [11, 60]. Also, nitrate
503 assimilation requires molybdenum in nitrate reductases [61], and Mo depletion in
504 Proterozoic oceans might have limited biologically available N supply to the surface
505 waters [29] where non-diazotrophic primary producers would depend on the vertical
506 mixing of ammonium released from organic matter in deep waters. In any case, our
507 simple scaling model establishes a framework for evaluating the evolving oceanic Mo
508 cycle and for illuminating Mo thresholds that biological experiments should explore
509 further.

510

511 **5.4 The emerging picture of Proterozoic ocean chemistry**

512 The $\delta^{98}\text{Mo}$ data from the 0.75 Ga Walcott Member are similar to those from 1.7
513 and 1.4 Ga black shales [56, 57] and provide evidence that sulfidic water masses
514 constituted the major sinks for Mo as recently as 750 Ma. Whether ocean euxinia was
515 persistent or recurrent remains uncertain and can only be assessed by continuing studies.

516 This finding is qualitatively consistent with current models which posit that the
517 expansion of free sulfide in subsurface water masses substantially reduced the Fe^{2+}
518 concentration in the deep ocean, diminishing the significance of banded iron formation

519 deposition from ~1.8 Ga until the later Neoproterozoic, when higher deep water Fe^{2+}
520 concentrations were reestablished and iron formations again deposited [46]. Our results
521 are also consistent with the emerging picture that while extensive, sulfidic conditions
522 were likely not global. Extensive sulfidic oxygen-minimum zone-like settings would
523 have been sufficient to account for the substantial removal of molybdenum and probably
524 also Fe^{2+} and a variety of other redox-sensitive trace metals. Proterozoic oceans may have
525 developed a complex redox structure distinguished by oxygenated surface waters, sulfidic
526 basins and settings similar to oxygen minimum zones with deeper ferruginous and
527 possibly even oxic waters in some places [7, 62, 63]. By 750-800 Ma ago, it appears that
528 sulfidic waters were more constrained by ferrous iron, perhaps developing only where
529 export of organic matter to subsurface water masses was high [7]. In any event, anoxic
530 and sulfidic water masses bathing continental shelves and platforms would have been
531 more stable if the atmosphere and oceans were less oxygenated. A low oceanic pO_2 , in
532 turn, helps to explain why marine animals with high O_2 requirements first diversified
533 after 750 Ma, near the very end of the Proterozoic Eon [7, 64]. While marine redox
534 indicators only constrain oceanic O_2 , and global marine oxygen depletion might
535 transiently occur even at high atmospheric O_2 levels [65], the persistence of low O_2 in
536 Proterozoic oceans is best explained by an overall low free O_2 inventory in the
537 atmosphere and ocean system before animals emerged on the planet.

538

539 **ACKNOWLEDGEMENTS**

540 We thank Carol Dehler for providing samples and Brian Kendall, Benjamin C.
541 Gill, David Johnston, and Bo Thamdrup for constructive discussions. Three anonymous

542 reviewers improved the manuscript. Funding was provided from the Danish National
543 Research Foundation (NordCEE), NASA Planetary Biology Internship, Villum Kann
544 Rasmussen foundation, and Danish National Research Agency (TWD) and NSF grant
545 EAR-0420592 (AHK).

546

547

- 549 [1] J. Farquhar, J. Savarino, S. Airieau, M.H. Thiemens, Observation of wavelength-
550 sensitive mass-independent sulfur isotope effects during SO₂ photolysis:
551 Implications for the early atmosphere, *Journal of Geophysical Research-Planets*
552 106(2001) 32829-32839.
- 553 [2] H. Holland, The oxygenation of the atmosphere and oceans, *Philosophical*
554 *Transactions of the Royal Society B: Biological Sciences* 361(2006) 903-915.
- 555 [3] J. Farquhar, H.M. Bao, M. Thiemens, Atmospheric influence of Earth's earliest
556 sulfur cycle, *Science* 289(2000) 756-758.
- 557 [4] D.E. Canfield, A. Teske, Late Proterozoic rise in atmospheric oxygen
558 concentration inferred from phylogenetic and sulphur-isotope studies, *Nature*
559 382(1996) 127-132.
- 560 [5] T.W. Dahl, E.U. Hammarlund, A.D. Anbar, D.P.G. Bond, B.C. Gill, G.W.
561 Gordon, A.H. Knoll, A.T. Nielsen, N.H. Schovsbo, D.E. Canfield, Devonian rise
562 in atmospheric oxygen correlated to the radiations of terrestrial plants and large
563 predatory fish, *Proc. Natl. Acad. Sci. U. S. A.* 107(2010) 17911-17915.
- 564 [6] D.E. Canfield, A new model for Proterozoic ocean chemistry, *Nature* 396(1998)
565 450-453.
- 566 [7] D.T. Johnston, S.W. Poulton, C. Dehler, S. Porter, J. Husson, D.E. Canfield, A.H.
567 Knoll, An emerging picture of Neoproterozoic ocean chemistry: Insight from the
568 Chuar Group, Grand Canyon, USA, *Earth Planet. Sci. Lett.* 290(2010) 64-73.
- 569 [8] P.F. Hoffman, D.P. Schrag, The snowball Earth hypothesis: testing the limits of
570 global change, *Terr. Nova* 14(2002) 129-155.
- 571 [9] A. Knoll, E. Javaux, D. Hewitt, P. Cohen, Eukaryotic organisms in Proterozoic
572 oceans, *Philosophical Transactions of the Royal Society B: Biological Sciences*
573 361(2006) 1023.
- 574 [10] K. Peterson, J. Cotton, J. Gehling, D. Pisani, The Ediacaran emergence of
575 bilaterians: congruence between the genetic and the geological fossil records,
576 *Philosophical Transactions of the Royal Society B: Biological Sciences*
577 363(2008) 1435.
- 578 [11] A.D. Anbar, Y. Duan, T.W. Lyons, G.L. Arnold, B. Kendall, R.A. Creaser, A.J.
579 Kaufman, G.W. Gordon, C. Scott, J. Garvin, R. Buick, A whiff of oxygen before
580 the Great Oxidation Event?, *Science* 317(2007) 1903-1906.
- 581 [12] L.E. Wasylenki, C.L. Weeks, T.G. Spiro, J.R. Bargar, A.D. Anbar, How Mo
582 isotopes fractionate during adsorption to Mn and Fe oxyhydroxides, Pergamon-
583 Elsevier Science Ltd, 2009, pp. A1419-A1419.
- 584 [13] J. Barling, A.D. Anbar, Molybdenum isotope fractionation during adsorption by
585 manganese oxides, *Earth Planet. Sci. Lett.* 217(2004) 315-329.
- 586 [14] L.E. Wasylenki, B.A. Rolfe, C.L. Weeks, T.G. Spiro, A.D. Anbar, Experimental
587 investigation of the effects of temperature and ionic strength on Mo isotope
588 fractionation during adsorption to manganese oxides, *Geochim. Cosmochim. Acta*
589 72(2008) 5997-6005.
- 590 [15] B.E. Erickson, G.R. Helz, Molybdenum(VI) speciation in sulfidic waters:
591 Stability and lability of thiomolybdates, *Geochim. Cosmochim. Acta* 64(2000)
592 1149-1158.

- 593 [16] T.W. Dahl, A.D. Anbar, G.W. Gordon, M.T. Rosing, R. Frei, D.E. Canfield, The
594 behavior of molybdenum and its isotopes across the chemocline and in the
595 sediments of sulfidic Lake Cadagno, Switzerland, *Geochim. Cosmochim. Acta*
596 74(2010) 144-163.
- 597 [17] C. Scott, T.W. Lyons, A. Bekker, Y. Shen, S.W. Poulton, X. Chu, A.D. Anbar,
598 Tracing the stepwise oxygenation of the Proterozoic ocean, *Nature* 452(2008)
599 456-459.
- 600 [18] S.R. Emerson, S.S. Huested, Ocean Anoxia and the Concentrations of
601 Molybdenum and Vanadium in Seawater, *Mar. Chem.* 34(1991) 177-196.
- 602 [19] J.L. Sarmiento, N. Gruber, *Ocean Biogeochemical Dynamics*, Princeton
603 university press, New Jersey, USA. 503 pp. (2006).
- 604 [20] G.R. Helz, E. Bura-Nakic, N. Mikac, I. Ciglenecki, New model for molybdenum
605 behavior in euxinic waters, *Chemical Geology*(2011).
- 606 [21] K.C. Biswas, N.A. Woodards, H. Xu, L.L. Barton, Reduction of molybdate by
607 sulfate-reducing bacteria, *Biometals* 22(2009) 131-139.
- 608 [22] M.D. Tucker, L.L. Barton, B.M. Thomson, Reduction of Cr, Mo, Se and U by
609 *Desulfovibrio desulfuricans* immobilized in polyacrylamide gels, *Journal of*
610 *Industrial Microbiology & Biotechnology* 20(1998) 13-19.
- 611 [23] M.D. Tucker, L.L. Barton, B.M. Thomson, Removal of U and Mo from water by
612 immobilized *Desulfovibrio desulfuricans* in column reactors, *Biotechnology and*
613 *Bioengineering* 60(1998) 88-96.
- 614 [24] T. Algeo, T. Lyons, Mo-total organic carbon covariation in modern anoxic marine
615 environments: Implications for analysis of paleoredox and paleohydrographic
616 conditions, *Paleoceanography* 21(2006) 1-A1016.
- 617 [25] N. Neubert, T.F. Nagler, M.E. Bottcher, Sulfidity controls molybdenum isotope
618 fractionation into euxinic sediments: Evidence from the modern Black Sea,
619 *Geology* 36(2008) 775-778.
- 620 [26] R.L.P. Brucker, J. McManus, S. Severmann, W.M. Berelson, Molybdenum
621 behavior during early diagenesis: Insights from Mo isotopes, *Geochemistry*
622 *Geophysics Geosystems* 10(2009) 25.
- 623 [27] J.L. Morford, S. Emerson, The geochemistry of redox sensitive trace metals in
624 sediments, *Geochim. Cosmochim. Acta* 63(1999) 1735-1750.
- 625 [28] J. McManus, W.M. Berelson, S. Severmann, R.L. Poulson, D.E. Hammond, G.P.
626 Klinkhammer, C. Holm, Molybdenum and uranium geochemistry in continental
627 margin sediments: Paleoproxy potential, *Geochimica Et Cosmochimica Acta*
628 70(2006) 4643-4662.
- 629 [29] A.D. Anbar, A.H. Knoll, Proterozoic ocean chemistry and evolution: A
630 bioinorganic bridge?, *Science* 297(2002) 1137-1142.
- 631 [30] C. Wheat, M. Mottl, M. Rudnicki, Trace element and REE composition of a low-
632 temperature ridge-flank hydrothermal spring, *Geochim. Cosmochim. Acta*
633 66(2002) 3693-3705.
- 634 [31] C. Archer, D. Vance, The isotopic signature of the global riverine molybdenum
635 flux and anoxia in the ancient oceans, *Nat. Geosci.* 1(2008) 597-600.
- 636 [32] C.R. Pearce, K.W. Burton, P. von Strandmann, R.H. James, S.R. Gislason,
637 Molybdenum isotope behaviour accompanying weathering and riverine transport
638 in a basaltic terrain, *Earth and Planetary Science Letters* 295(2010) 104-114.

- 639 [33] N. Neubert, A. Heri, A. Voegelin, T. Nögl, F. Schlunegger, I. Villa, The
640 molybdenum isotopic composition in river water: Constraints from small
641 catchments, *Earth and Planetary Science Letters*(2011).
- 642 [34] C. Siebert, T.F. Nagler, F. von Blanckenburg, J.D. Kramers, Molybdenum isotope
643 records as a potential new proxy for paleoceanography, *Earth Plan. Sci. Lett.*
644 211(2003) 159-171.
- 645 [35] J. Barling, G.L. Arnold, A.D. Anbar, Natural mass-dependent variations in the
646 isotopic composition of molybdenum, *Earth Planet. Sci. Lett.* 193(2001) 447-457.
- 647 [36] J.L. Hannah, H.J. Stein, M.E. Wieser, J.R. de Laeter, M.D. Varner, Molybdenum
648 isotope variations in molybdenite: Vapor transport and Rayleigh fractionation of
649 Mo, *Geology* 35(2007) 703-706.
- 650 [37] J. Martin, M. Meybeck, Elemental mass-balance of material carried by major
651 world rivers, *Mar. Chem.* 7(1979) 173-206.
- 652 [38] T. Goldberg, C. Archer, D. Vance, S.W. Poulton, Mo isotope fractionation during
653 adsorption to Fe (oxyhydr)oxides, *Geochim. Cosmochim. Acta* 73(2009) 6502-
654 6516.
- 655 [39] C.M. Dehler, M. Elrick, K.E. Karlstrom, G.A. Smith, L.J. Crossey, J.M.
656 Timmons, Neoproterozoic Chuar Group (similar to 800-742 Ma), Grand Canyon:
657 a record of cyclic marine deposition during global cooling and supercontinent
658 rifting, *Sediment. Geol.* 141(2001) 465-499.
- 659 [40] A.B. Weil, J.W. Geissman, R. Van der Voo, Paleomagnetism of the
660 Neoproterozoic Chuar Group, Grand Canyon Supergroup, Arizona: implications
661 for Laurentia's Neoproterozoic APWP and Rodinia break-up, *Precambrian Res.*
662 129(2004) 71-92.
- 663 [41] K.E. Karlstrom, S.A. Bowring, C.M. Dehler, A.H. Knoll, S.M. Porter, D.J. Des
664 Marais, A.B. Weil, Z.D. Sharp, J.W. Geissman, M.B. Elrick, J.M. Timmons, L.J.
665 Crossey, K.L. Davidek, Chuar Group of the Grand Canyon: Record of breakup of
666 Rodinia, associated change in the global carbon cycle, and ecosystem expansion
667 by 740 Ma, *Geology* 28(2000) 619-622.
- 668 [42] C.M. Dehler, M. Elrick, J.D. Bloch, L.J. Crossey, K.E. Karlstrom, D.J. Des
669 Marais, High-resolution delta C-13 stratigraphy of the Chuar Group (ca. 770-742
670 Ma), Grand Canyon: Implications for mid-Neoproterozoic climate change, *Geol.*
671 *Soc. Am. Bull.* 117(2005) 32-45.
- 672 [43] M.L. Williams, Crossey, L. J., Jercinovic, M. J., Bloch, J. D., Dehler, C. M.,
673 Heizler, M. T., Bowring, S. A., Goncalves, P., Dating Sedimentary Sequences: In
674 Situ U/Th-Pb Microprobe Dating of Early Diagenetic Mnazite and Ar-Ar Dating
675 of Marcasite Nodules: Case Study from Neoproterozoic Black Shales in the
676 Southwestern U.S., *GSA* 35, Seattle, 2003, p. p. 595.
- 677 [44] R.M. Nagy, S.M. Porter, C.M. Dehler, Y. Shen, Biotic turnover driven by
678 eutrophication before the Sturtian low-latitude glaciation, *Nat. Geosci.* 2(2009)
679 414-417.
- 680 [45] A. Hill, K. Cotter, K. Grey, Mid-Neoproterozoic biostratigraphy and isotope
681 stratigraphy in Australia, *Precambrian Res.* 100(2000) 281-298.
- 682 [46] D.E. Canfield, S.W. Poulton, A.H. Knoll, G.M. Narbonne, G. Ross, T. Goldberg,
683 H. Strauss, Ferruginous conditions dominated later neoproterozoic deep-water
684 chemistry, *Science* 321(2008) 949-952.

- 685 [47] G. Gordon, T. Lyons, G. Arnold, J. Roe, B. Sageman, A. Anbar, When do black
686 shales tell molybdenum isotope tales?, *Geology* 37(2009) 535-538.
- 687 [48] R. Raiswell, D.E. Canfield, Sources of iron for pyrite formation in marine
688 sediments, *Am. J. Sci.* 298(1998) 219-245.
- 689 [49] C.A. Partin, A. Bekker, C. Scott, B.C. Gill, T.W. Lyons, Changes in the
690 Precambrian ocean U cycle linked to the evolution of surficial redox conditions
691 AGU fall meeting 2009, Pergamon-Elsevier Science Ltd, San Francisco, 2009.
- 692 [50] J. McArthur, T. Algeo, B. van de Schootbrugge, Q. Li, R. Howarth, Basinal
693 restriction, black shales, Re-Os dating, and the Early Toarcian (Jurassic) oceanic
694 anoxic event, *Paleoceanography* 23(2008) PA4217.
- 695 [51] K.S. Habicht, M. Gade, B. Thamdrup, P. Berg, D.E. Canfield, Calibration of
696 sulfate levels in the Archean Ocean, *Science* 298(2002) 2372-2374.
- 697 [52] J.P. Hershey, T. Plese, F.J. Millero, The PK1-* for the Dissociation of H₂S in
698 Various Ionic Media, *Geochimica Et Cosmochimica Acta* 52(1988) 2047-2051.
- 699 [53] Y. Shen, D. Canfield, A. Knoll, Middle Proterozoic ocean chemistry: evidence
700 from the McArthur Basin, northern Australia, *Am. J. Sci.* 302(2002) 81-109.
- 701 [54] V. Brüchert, B. Currie, K.R. Peard, Hydrogen sulphide and methane emissions on
702 the central Namibian shelf, *Progress In Oceanography* 83(2009) 169-179.
- 703 [55] R. Robinson, P. Meyers, R. Murray, Geochemical evidence for variations in
704 delivery and deposition of sediment in Pleistocene light-dark color cycles under
705 the Benguela Current Upwelling System, *Marine Geology* 180(2001) 249-270.
- 706 [56] B. Kendall, R.A. Creaser, G.W. Gordon, A.D. Anbar, Re-Os and Mo isotope
707 systematics of black shales from the Middle Proterozoic Velkerri and
708 Wollogorang Formations, McArthur Basin, northern Australia, *Geochim.*
709 *Cosmochim. Acta* 73(2009) 2534-2558.
- 710 [57] G.L. Arnold, A.D. Anbar, J. Barling, T.W. Lyons, Molybdenum isotope evidence
711 for widespread anoxia in mid-proterozoic oceans, *Science* 304(2004) 87-90.
- 712 [58] A.L. Zerkle, C.H. House, R.P. Cox, D.E. Canfield, Metal limitation of
713 cyanobacterial N-2 fixation and implications for the Precambrian nitrogen cycle,
714 *Geobiology* 4(2006) 285-297.
- 715 [59] J. Glass, F. Wolfe-Simon, J. Elser, A. Anbar, Molybdenum-nitrogen co-limitation
716 in freshwater and coastal heterocystous cyanobacteria, *Limnology and*
717 *Oceanography* 55(2010) 667-676.
- 718 [60] M. Wille, J.D. Kramers, T.F. Nagler, N.J. Beukes, S. Schroder, T. Meisel, J.P.
719 Lacassie, A.R. Voegelin, Evidence for a gradual rise of oxygen between 2.6 and
720 2.5 Ga from Mo isotopes and Re-PGE signatures in shales, *Geochimica Et*
721 *Cosmochimica Acta* 71(2007) 2417-2435.
- 722 [61] R. Mendel, F. Bittner, Cell biology of molybdenum, *Biochimica et Biophysica*
723 *Acta (BBA)-Molecular Cell Research* 1763(2006) 621-635.
- 724 [62] J. Slack, T. Grenne, A. Bekker, O. Rouxel, P. Lindberg, Suboxic deep seawater in
725 the late Paleoproterozoic: Evidence from hematitic chert and iron formation
726 related to seafloor-hydrothermal sulfide deposits, central Arizona, USA, *Earth and*
727 *Planetary Science Letters* 255(2007) 243-256.
- 728 [63] S. Poulton, P. Fralick, D. Canfield, Spatial variability in oceanic redox structure
729 1.8 billion years ago, *Nat. Geosci.*(2010).

- 730 [64] C. Li, G.D. Love, T.W. Lyons, D.A. Fike, A.L. Sessions, X. Chu, A Stratified
731 Redox Model for the Ediacaran Ocean, *Science* 328(2010) 80-83.
- 732 [65] C.R. Pearce, A.S. Cohen, A.L. Coe, K.W. Burton, Molybdenum isotope evidence
733 for global ocean anoxia coupled with perturbations to the carbon cycle during the
734 early Jurassic, *Geology* 36(2008) 231-234.
- 735 [66] R. Mathur, S. Brantley, A. Anbar, F. Munizaga, V. Makshev, R. Newberry, J.
736 Vervoort, G. Hart, Variation of Mo isotopes from molybdenite in high-
737 temperature hydrothermal ore deposits, *Mineralium Deposita* 45(2010) 43-50.
- 738 [67] C. Siebert, T.F. Nagler, J.D. Kramers, Determination of molybdenum isotope
739 fractionation by double-spike multicollector inductively coupled plasma mass
740 spectrometry, *Geochemistry Geophysics Geosystems* 2(2001) art. no.-
741 2000GC000124.
- 742 [68] M.E. Wieser, J.R. de Laeter, A preliminary study of isotope fractionation in
743 molybdenites, *Int. J. Mass Spectrom.* 225(2003) 177-183.
- 744 [69] D. Malinovsky, D. Hammarlund, B. Ilyashuk, O. Martinsson, J. Gelting,
745 Variations in the isotopic composition of molybdenum in freshwater lake systems,
746 *Chemical Geology* 236(2007) 181-198.
- 747 [70] D. Malinovsky, I. Rodushkin, D. Baxter, J. Ingri, B. Öhlander, Molybdenum
748 isotope ratio measurements on geological samples by MC-ICPMS, *Int. J. Mass*
749 *Spectrom.* 245(2005) 94-107.
- 750 [71] A.J. Pietruszka, R.J. Walker, P.A. Candela, Determination of mass-dependent
751 molybdenum isotopic variations by MC-ICP-MS: An evaluation of matrix effects,
752 *Chemical Geology* 225(2006) 121-136.
- 753 [72] S.R. Taylor, S.M. McLennan, The Geochemical Evolution of the Continental-
754 Crust, *Rev. Geophys.* 33(1995) 241-265.
755
756
757

758 Figure 1: Histogram of $\delta^{98}\text{Mo}$ values in crustal samples including 86 molybdenites (mean
759 $\pm 1\text{sd}$: $0.36 \pm 0.54\text{‰}$), 6 subduction volcanites (mean $\pm 1\text{sd}$: $0.12 \pm 0.35\text{‰}$), and 7 granites
760 (mean $\pm 1\text{sd}$: $0.93 \pm 0.29\text{‰}$), respectively. Bin size is 0.15‰ set to 1 s.d. reproducibility of
761 the isotopic analysis, equivalent to $\pm 0.075\text{‰}$ (63% confidence interval). Data is compiled
762 from [33-36, 66-71].

763

764 Figure 2. Stratigraphic profile of the Chuar Group and relative water level (after [39]),
765 distribution of microfossils [44], bottom water redox conditions inferred from Fe
766 speciation data [after [7]] with expanded width indicating sample positions and
767 interpolated intervals.

768

769 Figure 3. Stratigraphy, distribution of microfossils, and local redox in the Upper Chuar
770 Group are shown as in Figure 2. Enrichments of highly reactive iron ($\text{Fe}_{\text{HR}}/\text{Fe}_{\text{T}} > 0.38$)
771 with high pyrite content [$\text{Fe}_{\text{P}}/\text{Fe}_{\text{HR}} > 0.7$] suggest deposition in a euxinic water column.
772 In contrast to modern euxinic sediments the Walcott member display low Mo, U, Mo EF,
773 U EF, and Mo/TOC below mean values of other Proterozoic sequences [17] implying
774 remarkably low Mo inventory in the Chuar basin. The uniform $\delta^{98}\text{Mo}$ ($\pm 2\sigma$
775 reproducibility) indicate persistently euxinic global oceans. Samples from Nankoweap
776 Butte are marked with a diagonal line (\), the rest are from Sixty Mile Canyon. Metal
777 enrichment factors are calculated by $\text{EF} = (\text{Mo}/\text{Al})_{\text{sample}}/(\text{Mo}/\text{Al})_{\text{av. crust}}$ using average
778 crustal values [72] to visualize authigenic enrichment and compensate for dilution by
779 carbonate sedimentation. Organic carbon content shown is LOI (in agreement with TOC
780 values from [41]).

781

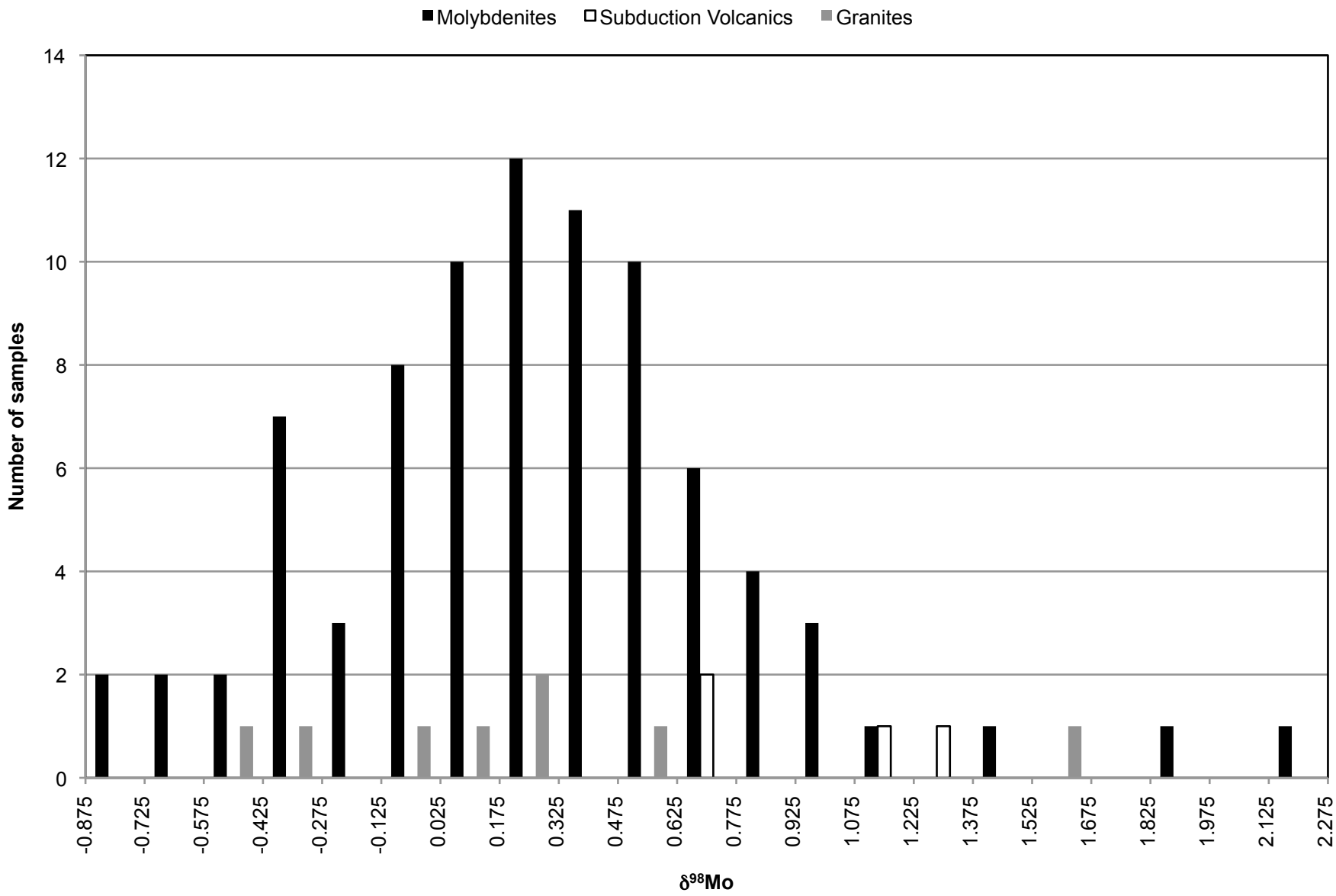
782 Figure 4. $\delta^{98}\text{Mo}$ is plotted as a function of Mo enrichment in the Walcott shales for
783 anoxic (■) and oxic (□) samples. Two samples have been oxidized in the outcrop (□,
784 dashed) and one sample has no Fe speciation data. The curve represents a mixing line
785 between lithogenic Mo with a crustal composition $\delta^{98}\text{Mo} = 0.7\text{‰}$ and authigenic,
786 unfractionated Mo with seawater at 1.0‰. Mo EF is used to measure the authigenic Mo
787 enrichment. Samples with high carbonate content are highlighted with accordingly low
788 siliciclastic fraction given in terms of $\text{Al}/\text{Al}_{\text{crust}}$ in %. The Mo contribution from
789 carbonate is insignificant ($[\text{Mo}]_{\text{carbonate}} \sim 0.02\text{-}0.07$ ppm) and can be ignored. Therefore,
790 Mo EF reflects authigenic enrichment in all samples.

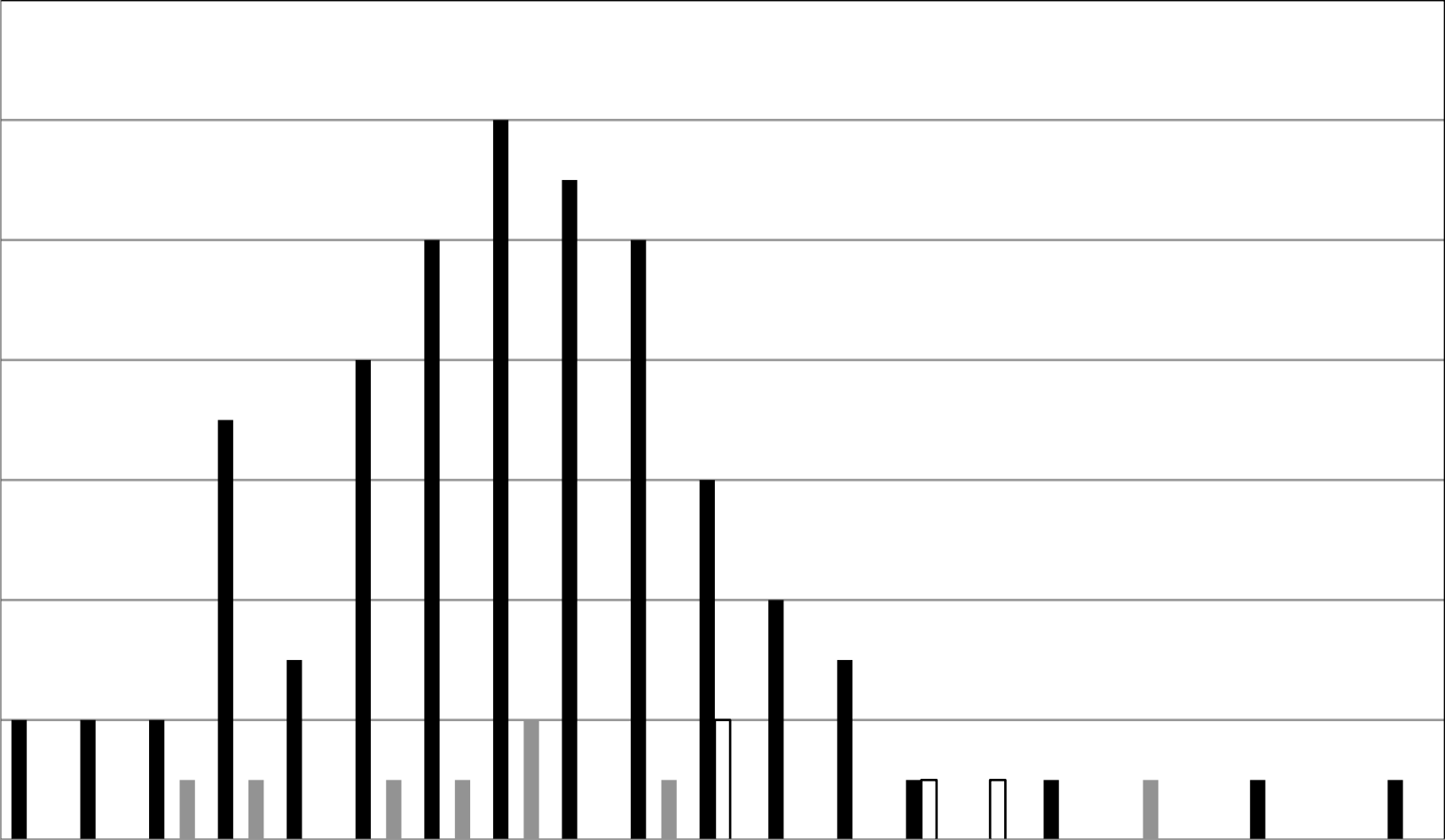
791

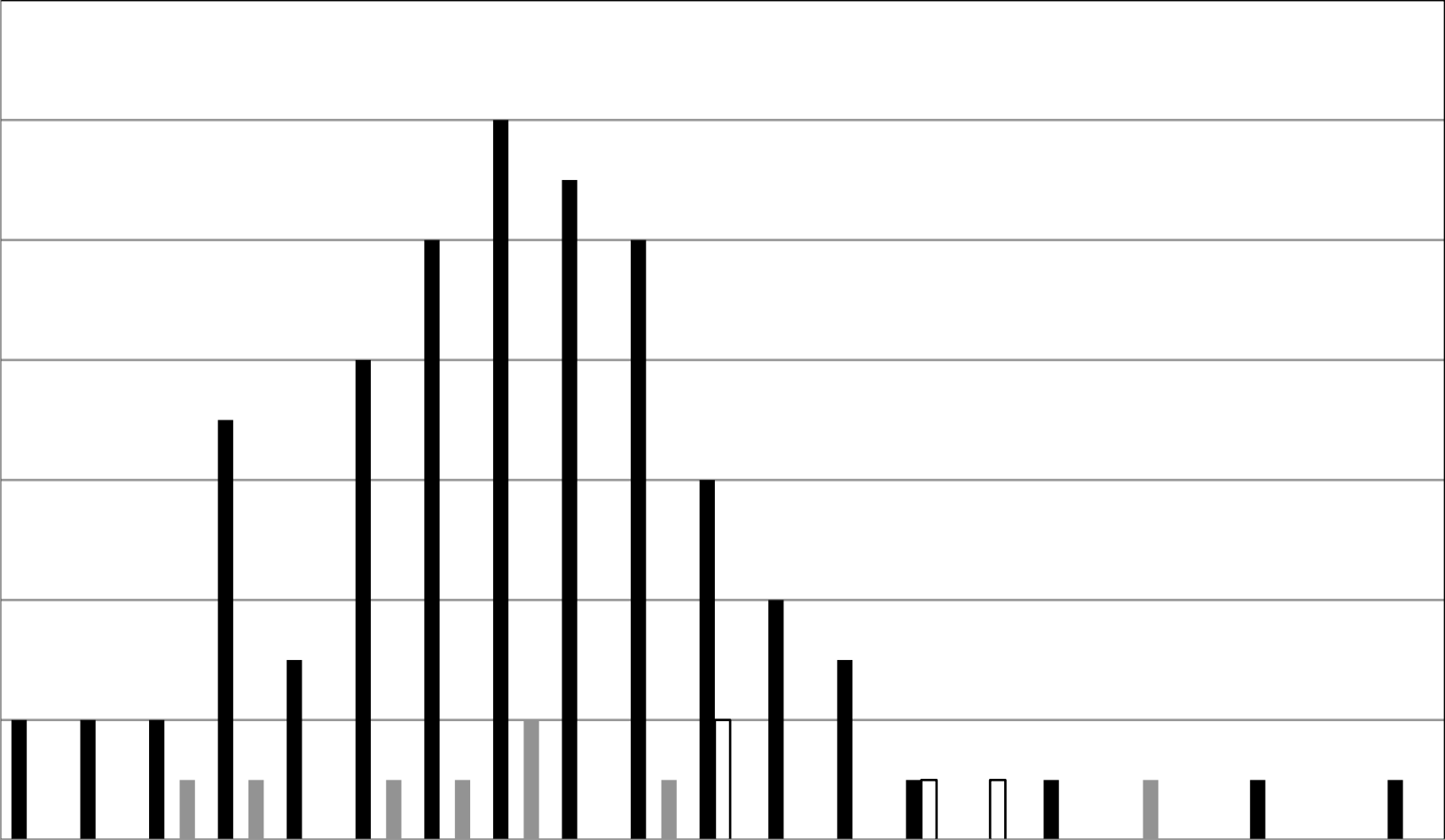
792 Table 1: Model predictions for the Mo residence time, seawater $[\text{Mo}]$ and $\delta^{98}\text{Mo}$ as a
793 function of various oceanic redox conditions assuming a direct response between Mo
794 inventory and burial rates ($y=1$). Examples of oceanic coverage are chosen to illustrate
795 how the parameters are related for various ocean compositions. Isotope values within the
796 Walcott range ($0.99 \pm 0.13\text{‰}$) are highlighted in red and bold. Parameter values
797 are: $\delta^{98}\text{Mo}_{\text{IN}} = 0.65\text{‰}$ [31], $\Delta_{\text{OX}} = -3.0\text{‰}$ [34], $\Delta_{\text{SAD}} = -0.7 \pm 0.2\text{‰}$ [26], $\Delta_{\text{EUX}} = 0\text{‰}$ [25],
798 $(r_{\text{EUX}}, r_{\text{SAD}}, r_{\text{OX}}) = (1.2, 0.2, 0.002) \mu\text{g cm}^{-2} \text{ yr}^{-1}$ and $F_{\text{IN}} = 1.8 \cdot 10^{10} \text{ g Mo/yr}$ [17], $\text{sf} =$
799 $\text{seafloor} = 3.6 \cdot 10^8 \text{ km}^2$.

800

801 Table 2: Sample locations and stratigraphic positions with Fe speciation distribution,
802 TOC, Al, Fe, Fe EF, Mo, Mo EF, Mo/TOC, $\delta^{98}\text{Mo}$, U, and U EF for black shales in the
803 Walcott Member of Chuar Group, Grand Canyon, USA.















Chuar Group Grand Canyon USA




Stratigraphy

-  shale
-  black shale
-  sandstone
-  dolomite
-  stromatolites
-  large crossbeds
-  subaerial exposure
-  physical unconformity

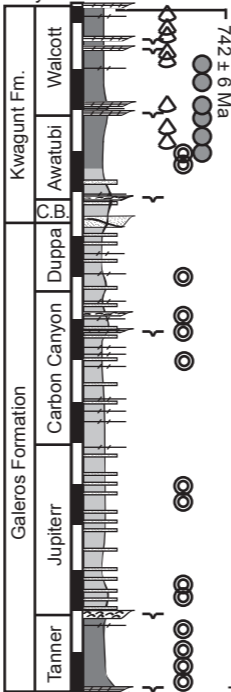
Fossil assemblages

-  vase shaped microfossils
-  diverse acritarchs
-  sphaerocongregus

Local redox

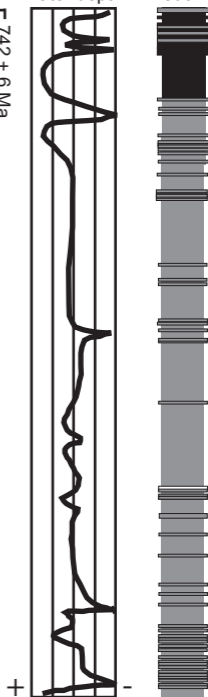
-  euxinic
-  ferruginous
-  oxic

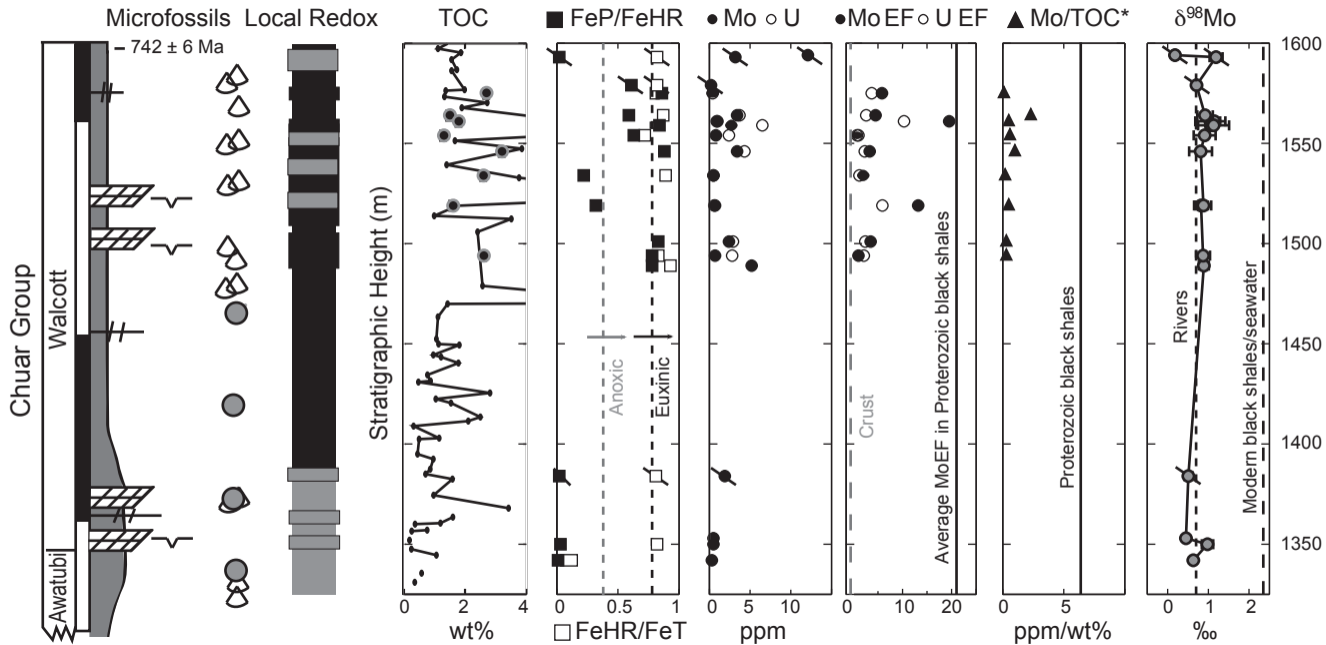
Sixty Mile Fm.

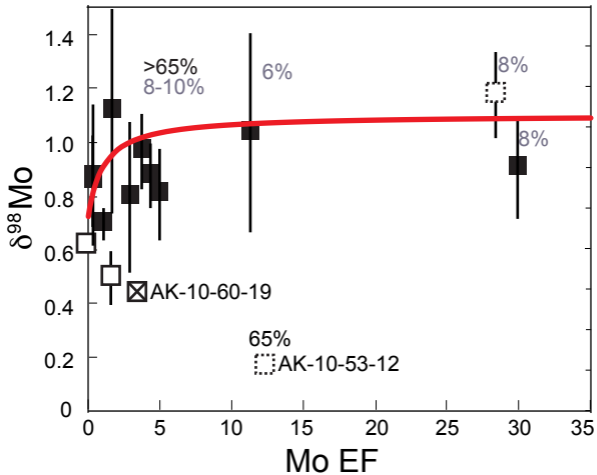


relative bottom water depth

redox







Direct feedback model	Euxinic % sf	Sulfidic at depth % sf	Oxic % sf	t_{Mo} [kyrs]	$[Mo]_{sw}$ [nM]	$\delta^{98}Mo_{sw}^c$ [‰]
Modern						
Scott et al. 2008 approx.	0.05	1	90	738	106	2.11 ± 0.10
Scott et al. 2008 (a)	0.063	1	87.5	721	104	2.04 ± 0.10
Brucker et al. 2009	0.021	1	112.5 ^b	724	105	2.35 ± 0.10
Kendall et al. 2009	0.021	1.2	87.5	725	105	2.12 ± 0.12
Ancient						
Euxinia 0.1%	0.1	1	0	972	140	1.12 ± 0.13
with oxic deep ocean	0.1	1	89	657	95	1.94 ± 0.09
with SS shelves	0.1	8	0	172	25	1.31 ± 0.17
with both	0.1	8	89	158	23	1.49 ± 0.17
Euxinia 0.3%	0.3	1	0	583	84	0.93 ± 0.08
with oxic deep ocean	0.3	1	89	453	65	1.54 ± 0.06
with SS shelves	0.3	8	0	154	22	1.24 ± 0.17
with both	0.3	8	89	143	20	1.41 ± 0.16
Euxinia 1.0%	1	1	0	243	35	0.77 ± 0.03
with oxic deep ocean	1	1	89	217	31	1.08 ± 0.02
with SS shelves	1	8	0	112	16	1.08 ± 0.12
with both	1	8	89	106	15	1.22 ± 0.11
Euxinia 2.0%	2	1	0	133	19	0.71 ± 0.02
with oxic deep ocean	2	1	89	124	18	0.91 ± 0.02
with SS shelves	2	8	0	81	12	0.96 ± 0.09
with both	2	8	89	78	11	1.06 ± 0.09
Euxinia 4.0%	4	1	0	69	10	0.68 ± 0.01
with oxic deep ocean	4	1	89	67	9.7	0.78 ± 0.01
with SS shelves	4	8	0	52	7.5	0.85 ± 0.06
with both	4	8	89	51	7.3	0.92 ± 0.05
Euxinia 8.0%	8	1	0	36	5.1	0.67 ± 0.01
with oxic deep ocean	8	1	89	35	5	0.72 ± 0.00
with SS shelves	8	8	0	30	4.4	0.77 ± 0.03
50% Euxinia	50	1	0	5.8	0.84	0.65 ± 0.00
with SS shelves	50	8	0	5.7	0.82	0.67 ± 0.01
90% Euxinia	90	1	0	3.2	0.47	0.65 ± 0.00
with SS shelves	90	8	0	3.2	0.46	0.66 ± 0.01

a) We re-calculate the exact areal coverage needed to balance the reported fluxes and parameter values used here.

b) The budget suggested by Brucker-Poulson et al. 2009 requires faster mean burial rate into oxic sediments.

c) The error estimate on $\delta^{98}Mo_{sw}$ represent the variation caused by varying $\Delta_{SAD} \pm 0.2\text{‰}$.

	Exposure ^{a)}	Strat. Height ^{b)} [m]	Fe _{HR} /Fe _T ^{c)}	Fe _{OX} /Fe _{HR}	Fe _{Mag} /Fe _{HR}	Fe _{Carb} /Fe _{HR}	Fe _P /Fe _{HR} ^{c)}	TOC wt%
AK-10-53-12	NB	1594	0.7	0.9	0.0	0.0	0.1	3.1
AK-10-53-13	NB	1593	0.8	1.0	0.0	0.0	0.0	2.5
AK-10-53-13A	NB	1579	0.8	0.1	0.0	0.3	0.6	6.4
AK-10-60-38	SMC	1575	0.8	0.1	0.0	0.0	0.9	7.3
AK-10-60-39	SMC	1564	0.9	0.2	0.0	0.2	0.6	14.4
AK-10-60-36	SMC	1561						27.8
AK-10-60-36 rep.	SMC	1561						
AK-10-60-35	SMC	1559	0.8	0.1	0.0	0.1	0.8	10.3
AK-10-60-35 rep.	SMC	1559						
AK-10-60-34	SMC	1554	0.7	0.3	0.0	0.1	0.6	1.7
AK-10-60-33	SMC	1546	0.9	0.1	0.0	0.1	0.9	6.8
AK-10-60-32	SMC	1534	0.9	0.3	0.0	0.5	0.2	13.7
AK-10-60-31	SMC	1519	1.0	0.3	0.0	0.4	0.3	16.3
AK-10-60-31 rep.	SMC	1519						
AK-10-60-30	SMC	1501	0.8	0.1	0.0	0.1	0.8	5.2
AK-10-60-29	SMC	1494	0.8	0.2	0.0	0.0	0.8	5.3
AK-10-60-28	SMC	1489	0.9	0.1	0.0	0.1	0.8	5.2
AK-10-53-15	NB	1384	0.3	0.7	0.0	0.2	0.1	20.7
AK-10-60-19	SMC	1353						0.4
AK-10-60-16	SMC	1350	0.8	0.8	0.0	0.2	0.0	7.9
AK-10-60-13	SMC	1342	0.1	0.7	0.1	0.2	0.0	0.6

^{a)} Sample localities are Sixty-Mile Canyon (SMC) and NE Flank of Nankoweap Butte (NB)

^{b)} Heights are given relative to the base of the Chuar Group as in (Dehler et al., 2001; Johnston et al., 2010).

^{c)} The local redox conditions are classified using Fe speciation data from (Canfield et al., 2008), where Fe_{HR}/Fe_T > 0.38 indicate deposition under anoxic waters, and Fe_P/Fe

^{d)} Al and Fe are obtained from XRF measurements (Canfield et al. 2008) assuming all Al and Fe are Al₂O₃ and Fe₂O₃, respectively.

^{e)} Metal enrichment factors are calculated by $X\ EF = (X/Al)_{\text{sample}} / (X/Al)_{\text{av. crust}}$ using average crustal values given above each column (Taylor and McLennan, 1995). Typical M This normalization compensates for variable dilution by carbonate sedimentation and facilitates visualization of authigenic enrichment.

^{f)} The $\delta^{98}\text{Mo} \pm \text{error}$ (n) are measured relative to the in-house Mo standard ("RochMo2") as described in a footnote of the main text.

Al ^{d)} wt%	Fe ^{d)} wt%	Fe EF ^{e)} (Fe/Al) _{crust} = 0.5 wt%/wt%	Mo ppm	Mo EF ^{e)} (Mo/Al) _{crust} = 0.19 ppm/wt%	Mo/TOC ppm/wt%	$\delta^{98/95}\text{Mo}$ ^{f)} ‰	U ppm	U EF (U/Al) _{crust} = 0.35 ppm/wt%
5.2	0.4	0.2	12.1	12.5	3.89	0.18 ± 0.02 (3)		
0.6	1.3	4.4	3.2	28.4	1.27	1.19 ± 0.16 (3)		
0.8	2.0	5.2	0.2	1.4	0.03	0.71 ± 0.06 (2)		
6.5	3.5	1.1	0.4	0.3	0.05		0.4	0.2
0.6	0.5	1.7	3.4	29.9	0.24	0.92 ± 0.19 (2)	3.7	17.4
0.5	0.4	1.8	1.0	11.5	0.04	1.05 ± 0.37 (3)	0.9	5.5
						1.15 ± 0.14 (2)		
7.4	4.7	1.3	2.7	2.0	0.26	1.13 ± 0.38 (2)	6.5	
						1.06 ± 0.12 (3)		
6.1	1.6	0.5	0.8	0.7	0.48	0.91 ± 0.27 (3)	2.4	1.1
5.7	3.1	1.1	3.4	3.2	0.50	0.81 ± 0.28 (3)	4.3	2.1
0.8	0.9	2.3	0.5	3.4	0.04		0.5	1.8
0.7	0.7	2.1	0.7	5.3	0.04	0.82 ± 0.17 (2)	0.6	2.4
						0.88 ± 0.19 (2)		
5.6	2.7	1.0	2.4	2.3	0.46		2.9	1.5
5.9	2.8	0.9	0.7	0.6	0.13	0.87 ± 0.17 (3)	2.8	1.4
6.0	3.5	1.1	5.2	4.6	1.00	0.89 ± 0.12 (3)		
5.4	1.5	0.6	1.9	1.9	0.09	0.51 ± 0.10 (3)		
0.7	0.2	0.5	0.5	3.7	1.25	0.45 (1)		
0.7	0.8	2.4	0.5	4.0	0.06	0.98 ± 0.14 (3)		
9.1	1.4	0.3	0.3	0.2	0.53	0.63 ± 0.03 (2)		

$\text{HR} > 0.7-0.8$ distinguish anoxic+sulfidic bottom waters from anoxic + ferruginous waters.

lo EF values for Archean- and Proterozoic black shales are 2 and 21, respectively (Anbar et al., 2007).

Supplementary information to: Dahl et al. "Molybdenum evidence for expansive sulfidic water masses..."

Electronic supplement to:

Molybdenum evidence for expansive sulfidic water masses in ~750 Ma oceans

T. W. Dahl, D. E. Canfield, M. T. Rosing, R. Frei, G. W. Gordon, A. H. Knoll, A. D. Anbar

A1: Modern Mo cycle

The modern oceanic molybdenum cycle has been constrained by isotopic mass balance of the major reservoirs (see main text and summaries in [1-3]). Here, we briefly summarize the state of knowledge necessary for the interpretation of the Mo isotopic composition in ancient sediments. Today, seawater carries a homogeneous isotope composition of $\delta^{98}\text{Mo} = 2.3 \pm 0.1\%$ [4-6] relative to the oceanic input of dissolved Mo in rivers (90%) at $\sim 0.7\%$ [7-9]) with the rest from low temperature hydrothermal fluids [10] at $\sim 0.8\%$ [11].

A2 Mo cycle at 750 Ma

A2.1 Slow Mo accumulation in Chuar basin

Our interpretation rests on the assumption that the Walcott basin was capable of rapid, euxinic accumulation of molybdenum. We therefore explore alternative options that could produce low trace metal abundances (Mo = 1-12 ppm, U = 1-7 ppm, Mo/TOC ~ 0.5 ppm/wt%) contrasting high Mo enrichments in modern sediments deposited under similar conditions (Table S1).

	Deep water $\Sigma S(-II)^{aj}$	Deep-water [Mo] _{aq} salinity corrected nM	Deepwater [Mo] normalized to seawater	Bulk sed. acc. rate $g\ cm^{-2}\ yr^{-1}$	organic C burial flux $mg\ cm^{-2}\ yr^{-1}$	Mo accumulation rate flux $nmol\ cm^{-2}\ yr^{-1}$	TOC wt%	Mo ppm	Mo/TOC ppm/wt %	$\delta^{98}Mo_s$ offset from surface water %
Black Sea, >400m depth	350	0.2-0.3	0.03-0.05	1-20	0.1-1	2	6.1	45	4.5	0 ^a
Framvaren Fjord	6000-8400	1.3-2.2	0.20-0.30	5-12	1.2-2.4	20	11.6	84	9	
Cariaco Basin	60	6.8-8.4	0.70-0.85	8-25	1-6	63	4.4	85	25	-0.7 to -0.4
Saanich Inlet	25	7.2-9.6	0.80-1.0	42-480	2-11	62	3.2	21	45	
Namibian Shelf	<10	10.5	1.00	12-80	1-10	16	6.7	33	6	
Walcott basin	6-2000	0.02		<14	0.1-0.6	0.33	1-4	2.2	0.2-0.9	

^{a)} Total sulfide: $\Sigma S(-II) = H_2S + HS^- + S^{2-}$

Table S1: Chemical characteristics of modern euxinic basins and inferred composition for the Walcott basin [20-22].

First, we test if the low Mo concentrations could be an artifact of exquisitely high sedimentation of Mo-depleted material. The average bulk sediment accumulation rate is derived from mean density ($2.7\ g\ cm^{-3}$) and sedimentation rate (1600 m / 30 Myrs) and gives $14\ mg\ cm^{-2}\ yr^{-1}$ for the entire Chuar basin. This is comparable to most other euxinic basins (Table S1) and might even overestimate the sedimentation rate during euxinic deposition, when sea level was at its highest and the water depth at its maximum. In combination with average Mo concentrations at 2.2 ppm, we estimate an average Mo accumulation rate of $0.33\ nmol\ cm^{-2}\ yr^{-1}$ for the Walcott shales. This overestimate is already 6-200 times slower than accumulation in modern euxinic basins.

Conclusively, the average bulk sedimentation rate is actually not high compared to modern euxinic sediments, and enhanced sedimentation of Mo-poor material could not produce observed low Mo

Supplementary information to: Dahl et al. "Molybdenum evidence for expansive sulfidic water masses..."

concentrations if the Walcott basin resembled a modern-type of euxinic system at the given mass accumulation rate.

Next, we test if conditions were in place for Mo accumulation to occur in the Walcott basin (hence solution 1 represent "no Mo capture"). In the current understanding of its euxinic burial pathway, molybdate is sourced from the surface ocean into the sulfidic deep waters and reacts with H₂S in three or four ligand exchange reactions to form the first and second strongly particle reactive oxythiomolybdate species, MoOS₃²⁻ and MoS₄²⁻ [23, 24], respectively. Trithiomolybdate is readily scavenged with sinking particles (organic matter or perhaps Fe-sulfides [25]) and preserved in the sediments. The current model for euxinic Mo accumulation has two general prerequisites, namely sinking particles and H₂S, and might also require Fe²⁺ and moderate pH levels ~6-8 [25]. Both organic matter and FeS/FeS₂ was settling out of the water column since 2-20 wt% total organic carbon and <2 wt% pyrite are present in the Walcott shales. The big question is whether particle reactive Mo species formed. Reactive MoOS₃²⁻ and possibly MoS₄²⁻ (given enough time or a catalytic reaction) are slowly produced from molybdate through reaction with H₂S. This takes place at H₂S > 10 μM [26]¹ equivalent to 40 μM total sulfide at Black Sea temperature and pH of 8°C and 7.69, respectively (remaining 30 μM is dissociated into HS⁻).

How sulfidic was the Walcott basin? Most of the highly reactive iron in the Walcott sediments precipitated as FeS/pyrite. Therefore, its precursor - amorphous FeS - must have formed through reaction with between Fe²⁺ and HS⁻ and, thus, the ion product was high: [Fe²⁺][HS⁻] > 10^{-2.95-pH} [27]. The continued euxinic signature in the Walcott shale suggests that pyrite production was limited by Fe²⁺ delivery and not by sulfide, so that [HS⁻] > [Fe²⁺]. In combination with the ion product, the equations combine to [HS⁻]² > [Fe²⁺][HS⁻] > (10^{-2.95-pH}) = (5 μM)². Hence, HS⁻

¹ The critical threshold above which trithiomolybdate forms in sulfidic waters is [H₂S] > K₀₃^{-1/3} = 10±2 μM. This is similar to the action point of switch for MoS₄²⁻ formation: H₂S > K₀₄^{-1/4} = K₀₄^{-1/4} = 11±3 μM (Erickson & Helz 2000).

Supplementary information to: Dahl et al. "Molybdenum evidence for expansive sulfidic water masses..."

concentrations higher than 5 μM can be inferred from basins where Fe-sulfides precipitate from the water column. This corresponds to total sulfide concentration $>7 \mu\text{M}$ (with 2 μM H_2S at $\text{pH} = 7.69$, $T = 8^\circ\text{C}$) and may well have yielded water column concentrations similar to sulfate concentration in the surface waters 1,000-4,000 μM (sulfate levels are discussed further below). Even mildly or intermittently euxinic basins at 0-60 μM total sulfide (Cariaco basin, Saanich Inlet and Namibian shelf, Table S1) display at least 10-fold higher Mo accumulation clearly distinct from our ~750 million year old shales, suggestive that low sulfide concentrations were not limiting sedimentary Mo accumulation in the Walcott basin. Further, if the new model for Mo accumulation is correct, Mo precipitation might even be limited in an alkaline basin if sulfide concentrations were too high [25]. One would have to argue that pH in deep euxinic waters were 0.3-0.7 units higher than observed in any modern euxinic basin, and further require permanently $> 1,000 \mu\text{M}$ total sulfide. Yet, Mo precipitation would proceed at intermediate sulfide concentration, for example near the chemocline, and may still preserve seawater $\delta^{98}\text{Mo}$ in some of the sediments. Conclusively, the only sensible explanation for the low Mo content and constant $\delta^{98}\text{Mo}$ value in the Walcott sediments is that the Mo concentration in contemporaneous seawater was low.

A2.2 Chuar basin - exploring solution space

We explore models that would explain the Mo and $^{98}\text{Mo}/^{95}\text{Mo}$ depletion in the Walcott basin.

Surface waters were charged with water, at rate V (m^3/s) from the ocean (SW) and local rivers plus continental runoff (R). Water is added through precipitation (P) and lost through evaporation (E), so that the abundance (M) and isotopic composition (δ) are given by:

equation 5

$$(V_R + V_{\text{SW}} + V_P - V_E) \text{Mo}_{\text{mix}} = V_R \cdot \text{Mo}_R + V_{\text{SW}} \cdot \text{Mo}_{\text{SW}}$$

equation 6
$$(V_R + V_{SW} + V_P - V_E) Mo_{mix} \cdot \delta_{mix} = V_R \cdot Mo_R \cdot \delta_R + V_{SW} \cdot Mo_{SW} \cdot \delta_{SW}$$

In steady state equations S1 and S2 combine to:

equation 7
$$0 = (\delta_R - \delta_{mix}) V_R \cdot Mo_R + (\delta_{SW} - \delta_{mix}) V_{SW} \cdot Mo_{SW}$$

and thus,

equation 7b
$$\begin{aligned} (\delta_{SW} - \delta_{mix}) \cdot Mo_{SW}/Mo_R \cdot V_{SW}/V_R &= (\delta_{mix} - \delta_R) \\ &= (\delta_{sed} - \delta_R) \\ &= 1.0 - 0.7 = \underline{0.3\text{‰}} \end{aligned}$$

In the second line, we assume that $\delta^{98}Mo$ of the Walcott sediments (sed) directly reflects the surface waters in the Walcott basin (mix), since there can be no isotope fractionation between sediments and water column when Mo is removed to extremely low Mo concentrations in the deep basin. Any of three factors on the left hand side of equation 7b need to be small. If the concentration and isotopic composition of contemporaneous seawater were similar to today (e.g. fully oxic oceans), the ratio of riverine to oceanic water discharge (V_{SW}/V_R) would need to have been 1/95.

Alternatively, the oceanic Mo cycle was dramatically different from today with seawater carrying much lower [Mo] and $\delta^{98}Mo$. Before we explore non-actualistic solutions (which implies globally expanded euxinia relative to today), we first discuss why riverine dilution in a hydrographically restricted basin (solution 2) is not a viable answer. The solution phenomena are described in table S2.

	Solution 1	Solution 2	Solution 3
Requirements	No Mo capture H ₂ S levels were permanently low	Riverine dilution Mixing ratio of oceanic to riverine fluids were 1:95.	Globally low $\delta^{98}\text{Mo}$, [Mo] $\delta_{\text{SW}} - \delta_{\text{CHUAR}} \sim 0.05\text{‰}$ $M_{\text{SW}}/M_{\text{R}} \sim 1$
Implication	Possible Modern Oxidic Oceans	Possible Modern Oxidic Oceans	Widespread Anoxia
Problems	Fe speciation evidence for high $[\Sigma\text{S}(-\text{II})]$	Unrealistic restriction and $S_{\text{SW}} > 14 \text{ mM}$	(Remarkably low [Mo] and $\delta^{98}\text{Mo}$)

Table S2: Phenomena that may lead to low Mo and $\delta^{98}\text{Mo}$ in a euxinic basin

A2.2.1 Solution 2: Riverine dilution and globally oxic oceans

It has been suggested that the low $\delta^{98}\text{Mo}$ values in the Toarcian black shales of the Cleveland basin (~180 Ma) reflects basinal dilution with riverine fluids [28], and we outline four lines of evidence why such a scenario is insufficient to explain our results from the Chuar basin.

1) Local sea level increased markedly during Walcott times [19], and the connection to the open ocean was likely at its maximum during times of basinal euxinia. This conforms to independent lines of evidence for a marine deposition environment, which are summarized in the main text (including the globally significant microfossil assemblage observed in many other marine basins worldwide).

2) The geometry and hydrographic conditions of the Chuar basin are not well known, but when comparing to the required mixing ratio of seawater to riverine discharge (1:95) to modern marine-connected basins, we can find no modern analogue with similar freshwater dilution. The modern Baltic Sea display deep water salinities of ~10 g/L (25% oceanic component), far from the

Supplementary information to: Dahl et al. "Molybdenum evidence for expansive sulfidic water masses..."

required setting where 98.9% water is sourced from rivers and only 1.1% from the ocean (Salinity = 0.36).

3) Fluid dynamic considerations elucidate why marine basins contain substantial input of ocean water. Water bodies near the coast that form when fresh water from rivers mix with salt water from the ocean are called estuaries. In positive estuaries (most estuaries), riverine discharge exceeds evaporation allowing for stable salinity gradient and density stratification in the water column. At steady state, surface salinity provides a measure of the mixing ratio of these sources. The complementary "negative estuaries" (e.g. the Mediterranean) display efficient evaporation that drives surface water more saline and leads to an inverted density gradient promoting convective mixing in the basin. For our purpose, negative estuaries can be disregarded since the sediments would record Mo sourced directly from the saline surface waters (inconsistent with a fully oxic Mo cycle) and contradict observed anoxic deep waters unless atmospheric oxygen levels were lower than today.

To maintain stable stratification in a positive estuary saline water must have been supplied to the deep Chuar basin. This stratification is at odds with the extreme supply of river water that is needed in order to generate deceptively low Mo and $\delta^{98}\text{Mo}$ in the basin and produce a contrasting composition to the open ocean. The criterion for estuarine stratification is summarized in the estuarine Richardson number, which defines the ratio of the stabilizing effect of stratification and the destabilizing effect of shear:

equation 8
$$\text{Ri}_E = (g \cdot \Delta\rho \cdot V_R) / (\rho \cdot W \cdot U^3)$$

g - gravity; $\Delta\rho$ - density difference between seawater and freshwater; V_R - riverine water flux, ρ = density in the deep basin, W - characteristic width of the estuary, U - r.m.s. tidal velocity.

Estuaries are stably stratified at $Ri_E > 0.8$ [29]. This occurs at high riverine water flux (V_R) and substantial density gradient between its freshwater and seawater sources ($\Delta\rho$). Stable stratification requires a massive riverine discharge of $V_R > 250 \text{ m}^3/\text{s}$ comparable to the Maule River in Chile or three times the Hvítá River [$80 \text{ m}^3/\text{s}$, (Pearce et al. 2010)] in Iceland (here, we assumed the following parameters values: $\Delta\rho = 35 \text{ kg cm}^{-3}$, seawater density $1,035 \text{ kg m}^{-3}$, $g = 9.8 \text{ m/s}^2$, $W > 10 \text{ km}$, $U > 0.22 \text{ m/s}$). The shape of the Chuar basin is unknown, but the minimal lateral width for the Chuar basin (W) is given from today's exposure, 10 km [19]. There is no sedimentological evidence for major fluvial deposits. In fact, tidal influence is reported throughout the section [19] suggestive of a low estuarine Richardson number.

Lastly, we note that a steady undercurrent is driving seawater to any positive estuarine basin. This bottom-water flow is maintained by the horizontal pressure gradient that develops as riverine fresh water entrains into deeper saline waters while dragging basinal waters towards the ocean. The process maintains a landwards undercurrent refilling the deep part of the basin. Consequently, molybdate is sourced from the open ocean into the deeper part of positive estuarine basins even in hydrographically restricted basins. This model provides an explanation why highly euxinic sediments in remote marine basins, such as the deep Black Sea, still carry $\delta^{98}\text{Mo}$ of global seawater [21], and encourages the use of Mo isotopes to track global ocean redox conditions in the past from restricted marine basins.

4) The hydrographic restriction hypothesis is further disqualified when considering the sulfur cycle in the basin, because the sulfate concentrations in the ocean would need to have been much higher than previously reported. The presence of sulfur isotope fractionation between exported pyrite and carbonate associated sulfate in the Walcott basin [30] implies that the basinal

sulfate concentrations were $> 200 \mu\text{M}$ [31]. Concentrations are much lower in unpolluted rivers ($\sim 50 \mu\text{M}$), and so sulfate must have been sourced from a more concentrated reservoir, almost certainly from the ocean. A simple model for the sulfur cycle in the Chuar basin (Figure S2) allows us to evaluate, what the sulfate concentration in the oceanic source would need to have been at the extreme freshwater dilution needed to fulfill the molybdenum constraint (equation 7b).

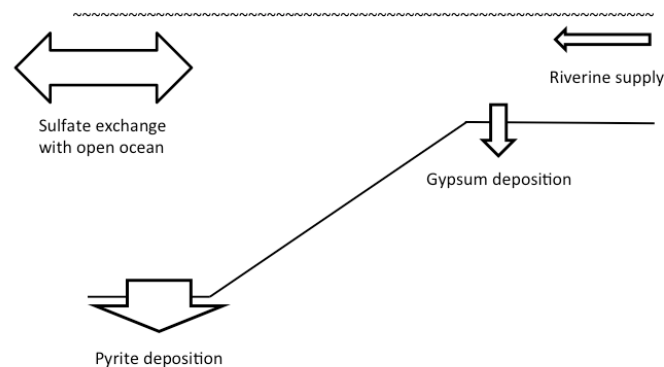


Figure S1: Simplified sulfur cycle in the Chuar basin when evaporation and precipitation balance each other. Continental runoff is negligible due to very low sulfate concentrations in river water.

The sulfate concentration in surface waters, S_{mix} , is determined by the concentration in the oceanic (S_{SW}) and riverine (S_{R}) sources and the corresponding water discharge (q_{SW} , q_{R}), precipitation (P) and evaporation (E):

equation 9:
$$(q_{\text{R}} + q_{\text{SW}} + P - E) S_{\text{mix}} = q_{\text{R}} S_{\text{R}} + q_{\text{SW}} S_{\text{SW}}$$

Supplementary information to: Dahl et al. "Molybdenum evidence for expansive sulfidic water masses..."

In positive estuaries $E \approx P \ll q_R, q_{SW}$ so the sulfur (eq. 5) and molybdenum (eq. 3) constraint yields: $S_{SW} = S_{mix} (q_R / q_{SW} + 1) - q_R / q_{SW} \cdot S_R > 0.2 \text{ mM} (95 + 1) - 95 \cdot 0.05 \text{ mM} > 14 \text{ mM!}$

This is again a minimum estimate. Still, seawater sulfate concentration should have been ~1 order of magnitude higher than previously reported for Proterozoic seawater (0.5-4 mM [30, 32]). We conclude that also in this view is the restriction model unattractive as it directly contradicts with previous attempts to quantify sulfate concentration in Proterozoic oceans.

A2.2.2 Solution 3: Globally anoxic oceans

The only reasonable solution, to the observed low sedimentary [Mo] and $\delta^{98}\text{Mo}$ in the Walcott shale, is that their associated values in contemporaneous seawater were significantly lower than today (solution 3). This will occur when sulfidic water masses are expanded globally at the expense of oxic seafloor that we know from modern oceans. Both $\delta^{98}\text{Mo}$ and Mo concentration in seawater decrease as H_2S becomes globally abundant (Table 1). Therefore, expanded euxinia worldwide is an attractive solution. A simple model for oceanic Mo and $\delta^{98}\text{Mo}$ is described in the model section in the main text. We find realistic solutions for the oceanic Mo budget at 750 Ma at substantial anoxia corresponding to anoxic waters covering a large proportion of the continental shelf sediments.

A2.2.2.1 Mathematical derivation of the direct feedback model

The Mo inventory in the ocean changes with time according to equations 1-4 in the main text:

equation 1
$$d\text{Mo}/dt = F_{\text{sources}} - F_{\text{sinks}}$$

equation 2
$$F_{\text{SINKS}} = F_{\text{OX}} + F_{\text{SAD}} + F_{\text{EUX}}$$

equation 3
$$F_i = A_i \cdot r_i \quad i = \text{OX, SAD, or EUX.}$$

equation 4
$$r_i = r_{i,\text{today}} \cdot \text{Mo}/\text{Mo}_{\text{today}}$$

The combination of equation 1-4 leads to a simple 1st order differential equation:

equation 10
$$d\text{Mo}/dt = a - b \cdot \text{Mo}$$

Supplementary information to: Dahl et al. "Molybdenum evidence for expansive sulfidic water masses..."

where a and b are functions only of areal coverage of each redox environment. The solution is that the Mo inventory changes from its initial inventory, Mo_0 , in an exponentially decreasing manner towards a "terminal Mo inventory", Mo_{term} :

equation 11
$$Mo(t) = Mo_{term} + (Mo_0 - Mo_{term}) \cdot \exp(-t/\tau)$$

Any short-term perturbation on Mo is damped over a characteristic time scale known as the residence time scale (τ) and relaxes at a terminal Mo inventory (Mo_{term}) given by:

equation 12
$$Mo_{term} = a/b = F_{sources} \cdot \tau$$

equation 13
$$\tau = b^{-1} = \kappa^{-1} \cdot \tau_{today}$$

Here, κ is the burial forcing function that is given in terms of areal extent of each redox environment, and the modern values used in the scaling laws. Combining equations 1-4 and 10-13 yields:

equation 14a
$$a = F_{source}$$

equation 14b
$$b = (A_{OX} \cdot r_{OX} + A_{SS} \cdot r_{SS} + A_{EUX} \cdot r_{EUX}) / ([Mo]_{today} \cdot V_{today})$$

Substituting parameter values from [3] gives a forcing function:

equation 15
$$\begin{aligned} \kappa = b \tau_{today} &= (A_{OX} \cdot r_{OX} + A_{SS} \cdot r_{SS} + A_{EUX} \cdot r_{EUX}) / F_{SINKS} \\ &= 0.367 (a_{OX}/90\%) + 0.506 (a_{SAD}/1\%) + 0.127 (a_{EUX}/0.05\%) \end{aligned}$$

In the last line seafloor coverage is scaled to their estimated modern value and global Mo export covering $a_{OX} = 90\%$, $a_{SAD} = 1\%$ and $a_{EUX} = 0.05\%$ of the ocean floor ($\kappa = 1$) with burial rates, r_i , 0.021, 2.6 and 13 $nmol\ cm^{-2}\ yr^{-1}$, respectively [3]. Equation 15 highlights the potential importance

Supplementary information to: Dahl et al. "Molybdenum evidence for expansive sulfidic water masses..."

of the sulfidic sinks that would easily overrule the influence of the oxic removal pathway, if sulfidic water masses covered a substantial portion of the seafloor. Results are summarized in Table 1.

Literature cited

- [1] A.D. Anbar, O. Rouxel, Metal stable isotopes in paleoceanography, *Annual Review of Earth and Planetary Sciences* 35(2007) 717-746.
- [2] T.W. Dahl, E.H. Hammarlund, A.D. Anbar, D.P.G. Bond, B.C. Gill, G.W. Gordon, A.H. Knoll, A.T. Nielsen, N.H. Schovsbo, D. Canfield, A Devonian rise of atmospheric oxygen correlated to the radiations of terrestrial plants and predatory fish, *PNAS*(submitted).
- [3] C. Scott, T.W. Lyons, A. Bekker, Y. Shen, S.W. Poulton, X. Chu, A.D. Anbar, Tracing the stepwise oxygenation of the Proterozoic ocean, *Nature* 452(2008) 456-459.
- [4] Y. Nakagawa, M.L. Firdaus, K. Norisuye, Y. Sohrin, K. Irisawa, T. Hirata, Precise Isotopic Analysis of Mo in Seawater Using Multiple Collector-Inductively Coupled Mass Spectrometry Coupled with a Chelating Resin Column Preconcentration Method, *Analytical Chemistry* 80(2008) 9213-9219.
- [5] J. Barling, G.L. Arnold, A.D. Anbar, Natural mass-dependent variations in the isotopic composition of molybdenum, *Earth Planet. Sci. Lett.* 193(2001) 447-457.
- [6] C. Siebert, T.F. Nagler, F. von Blanckenburg, J.D. Kramers, Molybdenum isotope records as a potential new proxy for paleoceanography, *Earth Plan. Sci. Lett.* 211(2003) 159-171.
- [7] C. Archer, D. Vance, The isotopic signature of the global riverine molybdenum flux and anoxia in the ancient oceans, *Nat. Geosci.* 1(2008) 597-600.
- [8] C.R. Pearce, K.W. Burton, P. von Strandmann, R.H. James, S.R. Gislason, Molybdenum isotope behaviour accompanying weathering and riverine transport in a basaltic terrain, *Earth and Planetary Science Letters* 295(2010) 104-114.
- [9] N. Neubert, A. Heri, A. Voegelin, T. Nögl, F. Schlunegger, I. Villa, The molybdenum isotopic composition in river water: Constraints from small catchments, *Earth and Planetary Science Letters*(2011).
- [10] C. Wheat, M. Mottl, M. Rudnicki, Trace element and REE composition of a low-temperature ridge-flank hydrothermal spring, *Geochim. Cosmochim. Acta* 66(2002) 3693-3705.
- [11] J. McManus, T.F. Nagler, C. Siebert, C.G. Wheat, D.E. Hammond, Oceanic molybdenum isotope fractionation: Diagenesis and hydrothermal ridge-flank alteration, *Geochemistry Geophysics Geosystems* 3(2002).
- [12] J.L. Hannah, H.J. Stein, M.E. Wieser, J.R. de Laeter, M.D. Varner, Molybdenum isotope variations in molybdenite: Vapor transport and Rayleigh fractionation of Mo, *Geology* 35(2007) 703-706.
- [13] D. Malinovsky, D. Hammarlund, B. Ilyashuk, O. Martinsson, J. Gelting, Variations in the isotopic composition of molybdenum in freshwater lake systems, *Chemical Geology* 236(2007) 181-198.
- [14] D. Malinovsky, I. Rodushkin, D. Baxter, J. Ingri, B. Öhlander, Molybdenum isotope ratio measurements on geological samples by MC-ICPMS, *Int. J. Mass Spectrom.* 245(2005) 94-107.
- [15] R. Mathur, S. Brantley, A. Anbar, F. Munizaga, V. MaksaeV, R. Newberry, J. Vervoort, G. Hart, Variation of Mo isotopes from molybdenite in high-temperature hydrothermal ore deposits, *Mineralium Deposita* 45(2010) 43-50.
- [16] J. Martin, M. Meybeck, Elemental mass-balance of material carried by major world rivers, *Mar. Chem.* 7(1979) 173-206.
- [17] L.E. Wasylenki, B.A. Rolfe, C.L. Weeks, T.G. Spiro, A.D. Anbar, Experimental investigation of the effects of temperature and ionic strength on Mo isotope fractionation during adsorption to manganese oxides, *Geochim. Cosmochim. Acta* 72(2008) 5997-6005.

- [18] T. Goldberg, C. Archer, D. Vance, S.W. Poulton, Mo isotope fractionation during adsorption to Fe (oxyhydr)oxides, *Geochim. Cosmochim. Acta* 73(2009) 6502-6516.
- [19] C.M. Dehler, M. Elrick, K.E. Karlstrom, G.A. Smith, L.J. Crossey, J.M. Timmons, Neoproterozoic Chuar Group (similar to 800-742 Ma), Grand Canyon: a record of cyclic marine deposition during global cooling and supercontinent rifting, *Sediment. Geol.* 141(2001) 465-499.
- [20] T. Algeo, T. Lyons, Mo-total organic carbon covariation in modern anoxic marine environments: Implications for analysis of paleoredox and paleohydrographic conditions, *Paleoceanography* 21(2006) 1-A1016.
- [21] N. Neubert, T.F. Nagler, M.E. Bottcher, Sulfidity controls molybdenum isotope fractionation into euxinic sediments: Evidence from the modern Black Sea, *Geology* 36(2008) 775-778.
- [22] G.L. Arnold, A.D. Anbar, J. Barling, T.W. Lyons, Molybdenum isotope evidence for widespread anoxia in mid-proterozoic oceans, *Science* 304(2004) 87-90.
- [23] T. Vorlicek, M. Kahn, Y. Kasuya, G. Helz, Capture of molybdenum in pyrite-forming sediments: role of ligand-induced reduction by polysulfides 1, *Geochimica Et Cosmochimica Acta* 68(2004) 547-556.
- [24] T.W. Dahl, A.D. Anbar, G.W. Gordon, M.T. Rosing, R. Frei, D.E. Canfield, The behavior of molybdenum and its isotopes across the chemocline and in the sediments of sulfidic Lake Cadagno, Switzerland, *Geochim. Cosmochim. Acta* 74(2010) 144-163.
- [25] G.R. Helz, E. Bura-Nakic, N. Mikac, I. Ciglenecki, New model for molybdenum behavior in euxinic waters, *Chemical Geology*(2011).
- [26] B.E. Erickson, G.R. Helz, Molybdenum(VI) speciation in sulfidic waters: Stability and lability of thiomolybdates, *Geochim. Cosmochim. Acta* 64(2000) 1149-1158.
- [27] W. Stumm, J. Morgan, *Aquatic chemistry: chemical equilibria and rates in natural waters*, John Wiley & Sons, New York, NY 10158 (USA). 1995.(1995).
- [28] J. McArthur, T. Algeo, B. van de Schootbrugge, Q. Li, R. Howarth, Basinal restriction, black shales, Re-Os dating, and the Early Toarcian (Jurassic) oceanic anoxic event, *Paleoceanography* 23(2008) PA4217.
- [29] H. Fischer, Mixing and dispersion in estuaries, *Annual Review of Fluid Mechanics* 8(1976) 107-133.
- [30] D.T. Johnston, S.W. Poulton, C. Dehler, S. Porter, J. Husson, D.E. Canfield, A.H. Knoll, An emerging picture of Neoproterozoic ocean chemistry: Insight from the Chuar Group, Grand Canyon, USA, *Earth Planet. Sci. Lett.* 290(2010) 64-73.
- [31] K.S. Habicht, M. Gade, B. Thamdrup, P. Berg, D.E. Canfield, Calibration of sulfate levels in the Archean Ocean, *Science* 298(2002) 2372-2374.
- [32] Y. Shen, D. Canfield, A. Knoll, Middle Proterozoic ocean chemistry: evidence from the McArthur Basin, northern Australia, *Am. J. Sci.* 302(2002) 81-109.